The Effectiveness of Power Distribution Systems for Deployment on the Lunar Surface

Bradford Robertson *, Jeffrey McNabb †, Matthew Rines ‡, and Dimitri N. Mavris §
Aerospace Systems Design Laboratory, School of Aerospace Engineering, Georgia Institute of Technology, Atlanta, Georgia 30332

Douglas Stanley ¶
National Institute of Aerospace, Hampton, VA, 23666

Mool C. Gupta ‖
Department of Electrical & Computer Engineering, University of Virginia, Charlottesville, Virginia 22904, USA

Charles Taylor **
NASA Langley Research Center, Hampton VA 23681

Lunar habitation missions are currently being planned to have astronauts return to the moon by the mid 2020's with a sustained lunar presence by the end of the decade. The various landed modules needed to support the missions are expected to be distributed around Shackleton Crater at distances ranging from 1 to 15 km and with power needs ranging from 10 kW to 50 kW. Current plans call for a solar array to be installed on the rim of the crater that receives near-constant sunlight year around with a power distribution system that transfers power from the source to consumers. This paper details several power distribution systems: DC transmission lines, radio frequency power beaming, and optical power beaming. Sizing algorithms for each of these distributions systems along with their necessary subsystems were developed from literature and subject matter expertise input. Several experiments were then conducted to determine the performance of the systems along with their sensitivities to changes in assumptions for various sub-components. The defined Figures of Merit enable mission designers to select the best power distribution system for each possible power consumer mission scenario. The experimental results were analyzed and compiled into a set of figures that highlight the conditions for which a certain system outperforms the other.

Nomenclature

PDS	=	Power Distribution System
WPT	=	Wireless Power Transmission
$DDCU$	=	DC-to-DC Converter Unit
$ATCS$	=	Active Thermal Control System
SME	=	Subject Matter Expert
FOM	=	Figures of Merit
RF	=	Radio Frequency
DC	=	Direct Current
AC	=	Alternating Current
$SAVOR$	=	Solar Array Voltage Output Regulator
$VSAT$	=	Vertical Solar Array Technology

*Research Engineer II, ASDL, School of Aerospace Engineering, Georgia Tech, AIAA Member
†Graduate Research Assistant, ASDL, School of Aerospace Engineering, Georgia Tech
‡Graduate Research Assistant, ASDL, School of Aerospace Engineering, Georgia Tech
§S.P. Langley Distinguished Regents Professor and Director of ASDL, School of Aerospace Engineering, Georgia Tech, AIAA Fellow
¶President and Executive Director, National Institute of Aerospace, AIAA Associate Fellow
‖S.P. Langley Distinguished Professor, University of Virginia, National Institute of Aerospace, IEEE & OSA Fellow.
**Program Manager In-Space Assembly, NASA Langley Research Center

I. Introduction

The Artemis Program is committed to landing NASA astronauts on the Moon by 2024 and establishing a sustainable lunar presence by the end of the decade. Shackleton Crater is one of the proposed landing sites for the first set of missions as it provides numerous opportunities to evaluate various technologies and capabilities. Electrical power is required not only for those goals but other various mission support items such as communication equipment, habitation modules, autonomous rovers, and in-situ resource utilization. The current planned solution to the electrical power requirement is to deploy an array of solar panels on the rim of the crater that is illuminated for over 80% of the lunar orbit; however, the landed modules will need to be located at other places to carry out their respective functions [1] [2]. In order to transmit the power from the crater rim to the landed modules, a Power Distribution System (PDS) will be needed.

This study was commissioned to explore several distribution systems and quantify the estimated landed mass for each system along with evaluating against other metrics. The PDS's explored by this paper included a traditional DC power cable system and two wireless power transfer (WPT) systems: radio frequency (RF) power beaming, and optical power beaming. This study evaluated the entire conceptual design for each PDS including power electronics such as DC-to-DC Conversion Units (DDCU),the transmission equipment, Active Thermal Control Systems (ATCS), deployment systems, and support structures. Similar studies of lunar PDS have been executed in the past most notably Kerslake in 2008, but this study utilizes updated sizing methods for each of the subsystems derived from literature and subject matter experts (SMEs) [3]. In the Kerslake study, an AC power cable based PDSs were found to have a higher overall mass when compared to the DC power cables for the ranges of power and distances this study is analyzing [3].

The report is organized into seven sections including this introductory one. Section II provides an overview of power distribution systems and their necessary subsystems. Section III describes the algorithms and equations that were developed to size the PDS subsystems for this study. Section IV details the methods that were used to carry out the analysis and Section V containing the results of that analysis. Lastly, Section VI identifies avenues for future work in this area with Section VII providing the concluding remarks for this study.

II. Power Distribution Systems Overview

A PDS is a system that transmits electrical power from a power generation source to a power consumer. First, the electrical power is generated via a power plant; the power is then sent to a sub-station that conditions the power for transmission. Within the transmission sub-station, the voltage of the power is increased in order to reduce the transmission losses due to power dissipation via heat and other electrical effects. Once the transmitted power has arrived near the location of the power consumers, it enters another sub-station in which the voltage is lowered to an appropriate level for the power consumer to utilize. Once conditioned to the correct voltage level, the electrical power exits the PDS and is consumed. A terrestrial based example is illustrated by Figure 1 .

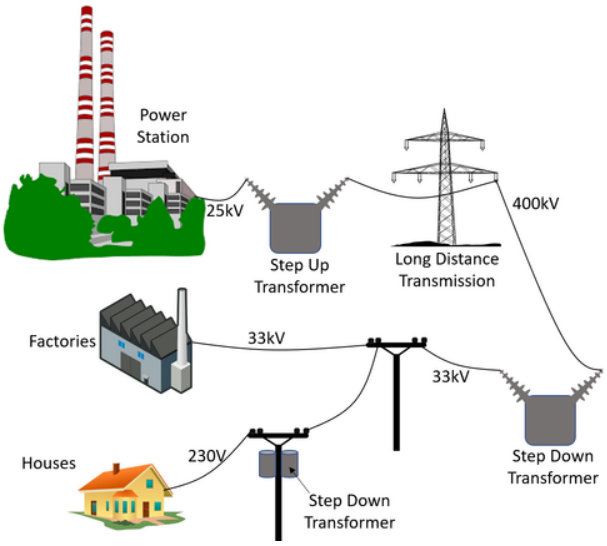

Fig. 1 Generic Earth Based Power Distribution System [4].

By taking a systems engineering based approach, this system can be functionally decomposed into a set of distinct blocks that each perform an unique function. This decomposition allows designers to quantify the impacts that changes to individual blocks have on the overall system. The functional decomposition of a PDS into discrete blocks is as follows: Power Generation, Pre-transmission Power Conditioning, Power Transmission, Post-transmission Power Conditioning, and Power Consumption. This is illustrated via the block diagram shown in Figure 2 .

Fig. 2 Functional Decomposition of a Generic Power Distribution System.

In order to size a PDS for Lunar deployment, each individual block needs to be sized and then summed in order to determine the estimated landed mass for each transmission method: DC power cables, RF power beaming, and Optical power beaming. On the lunar surface, there is no atmosphere to assist in the rejection of heat so all components must manage their thermal loads using radiation. This requirement couples together the component design with the design of its thermal control system. Figure 3 illustrates the functional decomposition of a lunar-based PDS and the individual blocks needed to be sized.

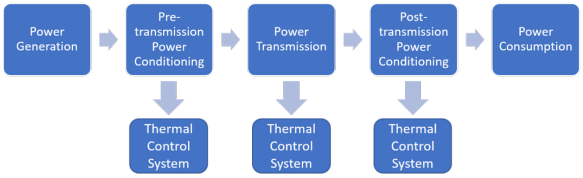

Fig. 3 Functional Decomposition of a Lunar Based Power Distribution System.

A. Lunar PDS Figures of Merits

A Figure of Merit (FOM) is a way for system designers to objectively compare the performance of a given system against an alternative. For this study, three total FOMs were used to evaluate the systems, one quantitative and two qualitative. The quantitative FOM was total landed system mass which captures the overall electrical efficiency of the system via the required number of power generators in addition to the system mass. The two qualitative FOMs,

Reliability and Maintainability & Operational Flexibility, are used by mission designers to assess the performance of the systems in areas where there are not explicit mathematical performance models. These FOMs are listed in Table 1.

Table 1 Figures of Merit

Figure of Merit	Description	Priority Level	Type	Technical Details
Landed Mass	The mass of the system required to be landed on the lunar surface to operate	1	Quantitative	$mass_{landed} = mass_{powerconditioning} + mass_{transmission} + mass_{thermalsystems} + mass_{deployment} + mass_{control} + mass_{powergeneration}$
Reliability and Maintainability	The availability of the power distribution system to provide power across operational conditions	2	Qualitative	Work with SMEs to determine at a high level, the overall system availability, ease of maintenance, required spares, and other operations or equipment that is needed to maintain the operability of the power distribution systems
Operational Flexibility	The ability for the system to provide power over a wide range of different operations for the end user(s)	3	Qualitative	Work with SMEs to determine the range of new operations enabled by each system and compare to baseline system.

III. Power Distribution System Sizing Algorithms

This section will detail how the sizing algorithms to estimate the total landed, system efficiency, and other performance measures. The sizing algorithms were developed through methods derived from literature review and with SME input. There were built upon the functional decomposition previously discussed; therefore, each sizing algorithm for the PDS is composed of five sub-routines that size their respective block. Additionally, each sizing algorithm was developed using the same iterative technique. This technique involves starting with an initial guess of the input power needed, then sizes the system and calculates the output power. If the calculated output power is less then the required power for a given case, the algorithm increases the input power needed. Once the correct input power has been determined, the algorithms add the calculated mass of the input power systems then stores the results into a database and proceeds to the next design case. The algorithm is furthered detailed in Figure 4 .

For this study, there are several common components across all the PDS's: power generation, power consumer, power conditioning, and the ATCS. The last two will be explained in greater detail in following sections as their are explicitly sized. The power generation and consumers will be held constant across this study in order to evaluate the performance of the different distribution methods directly against one another. The power generators will consist of an array of Vertical Solar Array Technology (VSAT) Project designs situated on the rim of Shackleton crater [5]. A VSAT is a relocatable solar capture device that deploys a set of solar panels from a mast so that they can be in a position to receive nearly continuous sunlight. Figure 5 illustrates how a VSAT tower is setup and deployed. Each VSAT tower can reach a deployment height of 16 meters and generates 10 kW with an estimated mass of 250 kg for the total system (legs, erector mechanism, control systems, mast, and solar panels) [5]¶. The power generated by an array of VSATs is assumed to be additive without loss. For example if it is determined that 100 kW of power is needed for a PDS then 10 VSAT towers are required for a total power generation mass of 2,000 kg. This mass is then added to the mass of the sized system to determine the total landed mass of a power distribution system. All power consumer blocks will be assumed to require a source voltage of 28 VDC [3] .

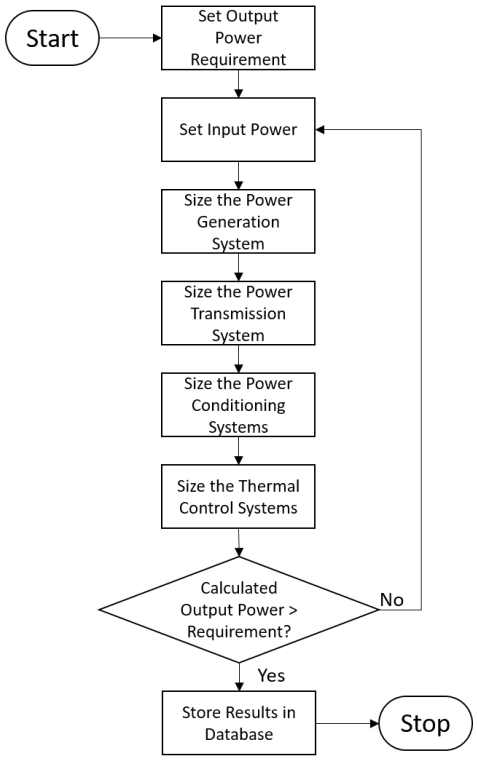

Fig. 4 Overall Structure and Logic of the Main Sizing Algorithm.

Fig. 5 VSAT Setup and Deployment [5].

A. Power Electronics Block Sizing

Power Electronics are the application of solid-state electronic systems to modify, control, and covert electrical power. For this study, they are used in both the pre and post-transmission power conditioning blocks to modify the voltage levels of the power. Since this study is limited to exploring DC based solutions, these blocks can be represented by DC-to-DC Converter Units (DDCU). The DDCUs are assumed to be a Weinberg topology which is the same design utilized on the ISS [6]. These are highly efficient units that can be designed to operate across a wide range of power and voltage levels [6].

The sizing algorithm used to size the DDCUs was adopted from a 2011 study conducted by Metcalf [7]. This study was an update to his previous works from 1992 and 2002 to account for new power electronic technology developments. For his study, Metcalf utilized data acquired from deployed space based power electronic subsystems to create parametric

sizing equations for each sub-system. These sub-systems can then be combined to create larger power electronics such as the DDCU along with a Solar Array Voltage Output Regulator (SAVOR) module. The SAVOR module is needed to control the output voltage and power from solar arrays found in both the power generation block for all PDS and the power transmission block for the Laser and blank systems.

Based on the document provided by Metcalf, a DDCU is composed of the following sub-systems: 2 DC Filters, DC-AC Inverter, AC Transformer, AC-DC Rectifier, DDCU Enclosure, Control Equipment, and Conductors. From this a general DDCU sizing algorithm was derived and is shown by Algorithm 1 . This algorithm sizes the estimated enclosure mass and thermal contact plates required to have a fully functional DDCU on the lunar surface. In order to save space only one example of the sub-system sizing algorithm will be detailed. The remaining algorithms can be found in detail in the paper by Metcalf [7]. The DDCU sizing algorithm takes in the input voltage, input power, and required output voltage; it then returns the estimated mass of the DDCU, estimated heat generated, and physical size of the DDCU. Two key assumptions are made in this algorithm. The first is that the DC filters and DC-AC Inverters will operate at a 40 kHz switching frequency which is the same switching frequency that the DDCUs onboard the International Space Station operate at. The second is that each sub-system within the DDCU will operate with a 3/2 redundancy. These means that there are 3 modules each rated to 50% of the input power which allow for the DDCU to operate at full power in the event of 1 module failure and 50% if a second fails within the same sub-system. This level of redundancy was determined to reduce the risk of DDCU failure to acceptable levels without incurring a significant mass penalty. Algorithm 2 details how the AC-DC Rectifier is sized. All other sub-systems are sized in a similar manner and the equations being developed by Metcalf [7] . The sub-component efficiencies were assumed to be state of the art since no source could be identified that demonstrated a significant technology improvement from when the Metcalf study was authored [7].

Algorithm 1: DDCU Sizing Algorithm

Input: Input Voltage, Input Power, Required Output Voltage
Output: Mass of DDCU, Size of DDCU, Heat Generated by DDCU

1 Size and compute Output Power of First DC Filter;
2 Size and compute Output Power of DC-AC Inverter ;
3 Size and compute Output Power of the AC Transformer;
4 Size and compute Output Power of AC-DC Rectifier;
5 Size and compute Output Power of Second DC Filter;
6 Size and compute Output Power of the Conductors and Control Systems;
7 Size the Enclosure ;
`/* Assume all power inefficiencies are converted directly to waste heat */`
8 heat generated = Input power - Output Power ;
9 Total Mass = Sum of All Component Masses

Algorithm 2: AC-DC Rectifier Sub-System Sizing Algorithm [7]

Input: Redundancy Factor, Input Power, Voltage In
Output: Mass of Inverter, Output Power

1 Rectifier Efficiency = 98.7% ;
2 Output Power = Rectifier Efficiency * Input Power ;
3 Rectifier Mass = $0.1175 \left[\frac{e^{\frac{0.005}{1-RectifierEfficiency}}}{1.469} * RedundancyFactor * OutputPower * \left(\frac{VoltageIn}{VoltageIn-2} \right)^6 \right]$;

B. Active Thermal Control System Sizing

A thermal control system is needed to dissipate heat from the various power distribution components to ensure they can continue to operate efficiently and meet their expected lifetimes. An active thermal control system was selected to be modeled since most of the power distribution components generate heat at a rate far higher than what a passive thermal control system could dissipate. Heat pipes are a common two-phase fluid flow system used in spacecraft that typically require no power to operate while operating at a high efficiency. Heat pipes can transport heat from a heat source, such as a coldplate that collects heat from a component, to a radiator that rejects heat to the environment. Although many

kinds of heat pipes exist, capillary-pumped loops and loop heat pipes are newer technologies [8]. They can maintain a narrow range of temperature control, tend to have lower mass than traditional heat pipe systems, and require no electrical power to operate [9]. For this study, the ATCS are designed using capillary-pumped loops. Figure 6 shows a schematic for a loop heat pipe system [10].

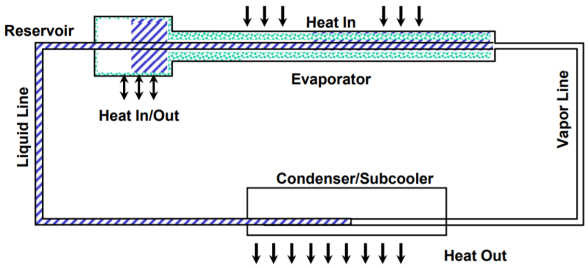

Fig. 6 Schematic of a loop heat pipe [10].

Algorithm 3 details the methodology used for sizing the ATCS. Individual systems are sized for every component of the power distribution system. The thermal control sizing is based on the worst-case or hot-case scenario, where the components are operating and in direct sunlight.

Algorithm 3: Sizing the Thermal Control System

Input: Heat generated, operating temperature, component dimensions
Output: Mass of thermal control system
Calculate incident and reflected solar radiation;
while |*radiatorArea - radiatorAreaNew*| > *1E-6* **do**
    Size the coldplate;
    Size the loop heat pipe;
    Size the radiator;
    Calculate incident and reflected solar radiation on the radiator;
    Resize the radiator;
end

1. Calculating the total heat to dissipate

The primary heat sources are the heat generated from the individual components, incident solar radiation, and reflected solar radiation from the lunar surface. The additional heat added due to thermal infrared radiation from the lunar surface is assumed to be negligible because the components will be resting on the surface with minimal exposed area facing the lunar surface. Similarly, heat conduction from the surface to the component is neglected because insulation will be built into the system. The generated heat from the component is calculated based on the component's power conversion efficiency, where all power lost to inefficiency is assumed to be converted into heat. The incident plus reflected solar radiation is calculated by Equation 1. It is assumed that half of the surface area of the component could be exposed to both incident and reflected solar energy. The component's surface finish is assumed to be high quality optical solar reflectors with 8 mil quartz mirrors with an absorptivity, α, of 0.05 [8]. The solar irradiance was set at 1414 W/m^2 which is the highest measured solar irradiance that occurs when the moon is in perihelion. The albedo of the lunar surface is taken to be 0.073 for calculating the reflected solar radiation [9].

$$SolarRadiation(W) = 1/2 \times A_{surface} \times \alpha \times irradiance_{solar} \times (1 + albedo) \tag{1}$$

2. Sizing the coldplate and radiator

The coldplate is sized assuming carbon-carbon material composition with an areal mass of 13.6 kg/m^2 [7]. The area of the coldplate is sized based on the largest planar area of the power distribution component. So, if there were a box

with dimensions 1 m × 2 m × 3 m, then the coldplate would be sized to one of the 2 m × 3 m faces and would have a mass of 13.6 kg/m^2 × 6 m^2 = 81.6 kg.

The radiator area is calculated via Equation 2, where Q is the heat needed to be dissipated [7]. The radiator is assumed to be two-sided, so $Num_{radiator-sides}$ equals 2. The temperature difference between the coldplate and the radiator is set to 11 K [7]. The coldplate temperature is assumed to be the same as the desired operating temperature of the component, and the sink temperature is set to 200 K [3] [11].

$$RadiatorArea(m^2) = \frac{\frac{1.0823E10}{Num_{radiator-sides}} \times Q}{(T_{coldplate} - \Delta T_{coldplate-to-radiator})^4 - T_{sink}^4} \quad [7] \quad (2)$$

Once the thermal control system is initially sized, the incident and reflected solar radiation impacting the radiator is calculated and the radiator is iteratively resized until it is large enough to expel the heat from the power distribution component and itself. The radiator is assumed to have the same surface finish as described for the power distribution component. The radiator areal mass is based on a carbon-fiber and aluminum honeycomb design with an embedded heat pipe condenser [12]. The radiator mass is given in Equation 3.

$$RadiatorMass(kg) = RadiatorArea(0.625 \times Num_{radiator-sides} + 1.25) \quad [12] \quad (3)$$

3. Sizing the loop heat pipe

Since the condenser mass is included in the radiator sizing, only the compensation chamber (labeled reservoir in Figure 6), evaporator, wick (located inside the evaporator), transport lines, and working fluid need to be sized. The material choices, diameters, and wall thicknesses are primarily based on empirical data of existing loop heat pipe systems [13] [14]. The evaporator, transport lines, and compensation chamber are made from stainless steel, while the wick is made of Nickel.

The evaporator was modeled with an outer diameter of 14.1 mm and a wall thickness of 2.7 mm. The evaporator length is sized to be the longer dimension of the coldplate. So from the previous coldplate example, it would be 3 m long. The transport lines have an outer diameter of 2.38 mm and a wall thickness of 0.63 mm.

The length of the transport lines are dependent on the distance the radiator is placed from the coldplate. A value of 5 m for the outgoing vapor line and returning liquid line was assumed for all cases. Because of their small size, the mass of the thermal control system is largely insensitive to their length. As a result the two transport lines are modeled with a mass of 0.08 kg each.

The wick is set to have an outer diameter equal to the inner diameter of the evaporator, 11.4 mm, and a length equal to the evaporator length. The porosity of the wick was selected to be 0.72. For simplicity, it is assumed that the vapor grooves are included in the porosity. Additionally, it is assumed to be a non-bayonet wick, so the inner diameter of the wick is equal to the inner diameter of the liquid line, 1.75mm.

The compensation chamber has an outer diameter of 22.2 mm and a wall thickness of 2 mm. The length is set to 324 mm so that the volume of the compensation chamber is equal to the largest volume in the empirical data [13]. The mass of the compensation chamber is therefore constant for all power distribution components at 0.171 kg.

The working fluid is chosen to be ammonia, which is commonly used for spacecraft applications including the ICESat-2's loop heat pipe [8] [10]. The mass of ammonia is scaled based on the relative volumes of the transport lines modeled here and of the ICESat-2. This results in a mass of 0.1 kg.

C. Power Cable Sizing

Power cables utilize a physical connection between the power generation source and the power consumer node. These connectors are made from electrically conductive materials such as copper. As stated earlier, this study is only exploring the use of DC-based power cables. The choice of DC cables simplifies the design of the cables and, as demonstrated by Kerslake's previous study, the transmission distances and power levels do not capture the benefits found on Earth based systems [3].

Figure 7 details the components that are needed for a lunar DC-cable based PDS. A design requirement for the DC power cables themselves is for them to be sized so that, when under load, they passively maintain their operating temperatures. This eliminates the need for the power cables for an ATCS to control their thermal output. Since this method of transmission requires a physical connection between two points, a deployment system must be accounted for to accurately estimate the landed mass. Algorithm 4 details the process for sizing the components and quantifying performance with the assumption that each end user will require a plug-in voltage of 28 V.

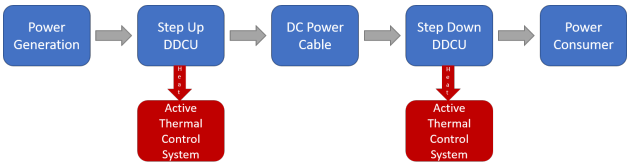

Fig. 7 Functional Decomposition of a Lunar DC Cable Power Distribution System.

Algorithm 4: Overall Power Cable System Sizing

Input: Power Out Required, Transmission Distance, Input Voltage
Output: Mass Breakdown, System Efficiency

```
for each Transmission Voltage do
    while not converged do
        Size Step-up DDCU and its ATCS ;
        Size the Power Cable ;
        Size Step-down DDCU and its ATCS ;
        Compute Support and Secondary Structure Mass ;
        Compute Deployment System Mass ;
        Increase Power Out for Next Iteration ;
    end
    Store Results in Database ;
end
Select Transmission Voltage that minimizes Overall System Mass
```

The outer for-loop in Algorithm 4 drives the analysis over a wide range of transmission voltages, 500 V to 10,000 V. This is done because, as the transmission voltage increases, the mass of the power cables decreases at the cost of increased mass of the insulation material and the power electronics. Thus, by exploring a large range of possible voltages at this stage, the algorithm is able to determine the best transmission voltage that minimizes the total mass of the PDS.

There are two additional calculations required to complete the overall power cable system sizing. These are the calculations to size the power cable and the deployment system. The power cable sizing algorithm was derived from a previous NASA study that explored the impacts of various power cable configurations, conductor material, and insulation material for use in DC power cables on the lunar surface [15]. From this study, a two-copper-cable configuration was used with one cable acting as the hot line (the power carrying line) and the other as a return line to complete the circuit. These cables would lie directly on the lunar surface and be deployed in a 2-fault tolerant manner meaning that a total of three pairs of cables will be connected between the Step Up and Step Down DDCUs. This decision was made by the authors to reduce the risk of total system failure due to electrical faults. Each cable consist of a copper conductor that is encased within a layer of PTFE insulation material. The cables (conductor and insulator) are sized in a manner that allows them to passively maintain a stable operating temperature given a lunar surface temperature of 250 K which was determined from analyzing the hottest surface temperatures in the proposed landing zone. A 10% routing factor was used to increase the length of the cables to account for any terrain traversals between the two connecting points. A bundle factor of 5% was added into total mass of the entire cable system (three cable pairs) to account for the mass of the cable spacers and other cable bundle hardware. A voltage drop of 5% was allowed in the cables in order to maintain a high system efficiency. Algorithm 5 details the general sizing algorithm used to evaluate the power cables.

Algorithm 5: Detailed Power Cable System Sizing

Input: Transmission Distance, Transmission Voltage, Input Power
Output: Cable Mass, Cable Power Loss, Cable Voltage Out, Cable Radius

Allowable Voltage Drop Fraction = 0.05 ;
Distance = (1+Routing Factor)*Transmission Distance ;
Current = Input Power / Transmission Voltage ;
Determine Initial Resistivity ;
while *not converged* **do**
    Update Resistivity ;
    Compute Cable Radius ;
    Compute Resistance ;
    Compute Voltage Drop ;
    Compute Cable Operating Temp ;
end
Insulation Thickness = Transmission Voltage /(Safety Factor * Insulator Breakdown Voltage) ;
Insulation Mass = $2*\pi*((\text{Insulation Thickness} + \text{Cable Radius})^2 - \text{Cable Radius}^2) * \text{Insulation Density} *$ Transmission Distance ;
Cable Mass = $2*\pi*\text{Cable Radius}^2 * \text{conductor density} * \text{Transmission Distance} + \text{Insulation Mass}$;
Cable Power Loss = Resistance * Current^2 ;
Cable Voltage Out = Transmission Voltage - Voltage Drop ;
Cable Bundle Mass = 3*Cable Mass * Bundle Factor

The resistivity of the wire can be assumed linear within the range of operating temperatures and can be approximated by the following equation:

$$\rho_{OperatingTemp} = \rho_{Material}\left[\frac{T_{Wire} + T_{o,material}}{293K + T_{o,material}}\right] \quad \text{[15]} \quad (4)$$

Where $\rho_{Material}$ is the initial resistivity of a material at 293 K and $T_{o,material}$ is the transition temperature of the material.

The cable radius can be found using the following equation:

$$r_{cable} = \sqrt{\frac{2 * InputPower * TransmissionLength * \rho_{OperatingTemp}}{\pi * VoltageDrop^2}} \quad \text{[15]} \quad (5)$$

The resistance within the cable can then be updated using the following formula:

$$R_{update} = \frac{\rho_{OperatingTemp} TransmissionLength}{\pi r_{cable}^2} \quad \text{[15]} \quad (6)$$

The Voltage Drop that occurs during transmission is calculated next using this equation where I is the current in the cable:

$$V_{drop} = IR_{update} \quad (7)$$

The new operating temperature can be found by solving the steady-state heat transfer equation assuming that half the wire radiates to deep space and the other half radiates into the surface.

$$T_{wire} = \left(\frac{1}{2}\left[\frac{I^2 R_{update} + 274.4 * r_{cable} * TransmissionLength}{\sigma \epsilon \pi F_{ws} * r_{cable} * TransmissionLength} + T_{surface}^4\right]\right)^{0.25} \quad \text{[15]} \quad (8)$$

In this equation, σ is the Stefan-Boltzman Constant, ϵ is the emissivity of the wire, F_{ws} is a configuration factor to account for the neighboring wire pair also radiating heat into the surrounding. F_{ws} was a constant introduced by Gordon from his study on lunar power cables and for this configuration was determined to be 0.818 [15].

The deployment system of the DC power cables is derived from work performed by NASA's Desert Research And Technology Studies (RATS) lunar surface human interaction evaluation program [16]. This program demonstrated

the technology needed to deploy a solar array and connect it via a power cable to an end consumer. Figure 8 shows the prototype cable deployment trailer. It consists of two main components: deployment trailer and cable reel. The deployment trailer was assumed to have a mass of 90 kg which is the mass of the prototype system. The size of the cable reel can be found solving for the flange diameter as shown by Figure 9 [17]. It is possible to use this equation because the cable reel's traverse is limited to 10 inches due to the trailer's physical design and the barrel diameter is assumed to be the minimum bending radius of the power cable. The National Electrical Code (NEC) and the Insulated Cable Engineers Association (ICEA) requirements for minimum cable bend radius limit the bend radius to 12 times the overall cable diameter [18] [19]. Equation 9 shows the reel sizing equation solved for flange diameter with the appropriate variable substitutions as detailed in Figure 9. The mass of the cable reel is then found via a regression model that was constructed off industrial cable reel mass data with the flange diameter as the independent variable.

$$FlangeDiameter = \left[\frac{15.3 * Length_{cable} * (2 * r_{cable})^2}{ReelTraverse} + (48 * r_{cable})^2\right]^{1/2} \quad [17] \quad (9)$$

Fig. 8 Prototype Power Cable Deployment Trailer [16].

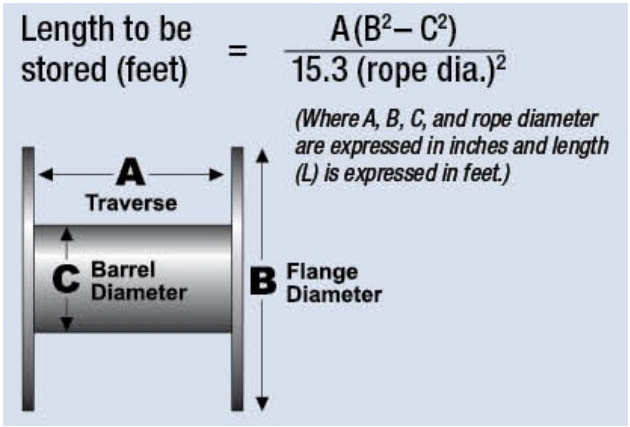

Fig. 9 Cable Reel Sizing Parameters [17].

D. RF Power Beaming

Radio Frequency Power Beaming utilizes electromagnetic waves between 2.45 GHz to 100 GHz to transmit power between two locations; however, this study only focused on three transmission frequencies: 2.45 GHz, 5.8 GHz, and 10 GHz. This choice was made because all components needed for higher frequencies are not at an appropriate technology readiness level to be considered for a mission launching within the next decade [20] . These components include the microwave generators and a specialized circuit called a rectifying antenna or rectenna. A rectenna is an antenna dipole combined with a rectifier in a single printed circuit and is essential for RF Power beaming as it converts the RF wave into electrical power [21] [20] .

Figure 10 details the required components needed to be sized for the RF Power Beaming system. The components that need to be sized are the microwave transmission antenna, the rectenna, and the microwave generators. Algorithm 6 details the sizing process for the components and quantifying performance.

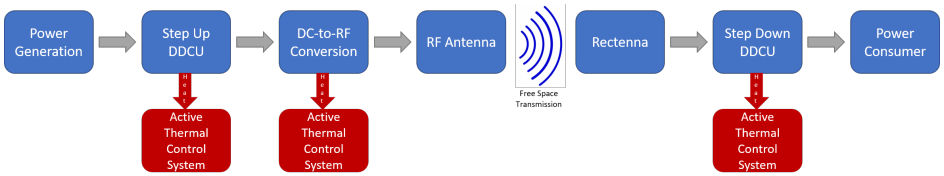

Fig. 10 Functional Decomposition of a Lunar RF Beaming Power Distribution System.

Algorithm 6: Overall RF Power Beaming System Sizing

Input: Power Out Required, Transmission Distance
Output: Mass Breakdown, System Efficiency
for *each Transmission Frequency* **do**
  Calculate Transmitted Power Requirement to Achieve Appropirate Power Density at Target Distance ;
  Size the Antenna ;
  Size the Rectenna ;
  Size the Microwave Generators and their ATCS ;
  Size the Step Up DDCUs and their ATCS ;
  Size the Step Down DDCU and its ATCS ;
end
return Mass Breakdown, System Efficiency ;

The Friis transmission equation is a fundamental formula in telecommunications and wireless power transfer studies as it relates the transmitted power and transmission antenna properties to the received power and receiving antenna properties. The equation is shown below:

$$\frac{P_r}{A_r} = \frac{P_t A_t}{d^2 \lambda^2} \quad \text{[22] (10)}$$

Where P_r is the power received at the antenna, A_r is the effective area of the receiving antenna, P_t is the transmitted power, A_t is the effective area of the transmission, d is the transmission distance and λ is the transmission wavelength. Due to changes in how modern day antennas are characterized, the equation has been rewritten to utilize antenna gain metrics to relate the transmitted power to the received power density at the target.

$$\Phi_r = \frac{P_t 10^{G/10}}{4\pi d^2} \quad \text{[22] (11)}$$

Where Φ_r is the received power density, G is the gain in decibels of the transmitting antenna, P_t and d are the same values as the last equation. From this equation it is now possible to solve for the required transmission power given one knows the needed power density, the transmission antenna gain, and the transmission distance.

A review of the available literature for RF Power beaming indicates that for the frequencies selected a power density of 100 W/m^2 is needed to achieve RF-to-DC conversion efficiencies of greater then 90% which is required to minimize

overall system mass [20] [23]. Higher efficiencies can be achieved by increasing the power density; however, this introduces a large safety risk to both human and robots operating in a nearby vicinity that could cross the beam's path.

Determining the gain of an antenna is a non-trivial task that was deemed outside the scope of this study; however, an appropriate gain is needed to carry out the calculations to size the system. A literature review was undertaken to find large scale system studies in which the gain of a transmission antenna was calculated. Throughout the 1970's and 1980's, NASA was tasked with evaluating the capabilities of a space-based power generation system that would transfer power from orbiting satellites to ground stations via microwaves [24] [25] [26] [27]. Numerous theoretical antenna design studies along with several technology demonstrations were completed during this time period. Each study recommend the use of a phased-array antenna composed of slotted wave-guides due to weight benefits, thermal performance, and an estimated antenna gain of 40 dBi [24] [25] [26] [27].

With the required transmitted power and antenna design known, the resulting antenna can be sized. The sizing algorithm for slotted antennas was derived from previous works conducted by El Misilmani et. al [28], Coburn et al [29], and Pandey [30]. Each individual slot antenna in the array was designed to radiate 1 kW of RF power at its design frequency, was assumed to be constructed of aluminum, and was able to passively control its temperature.

In order the size the rectenna, first the power output required from the rectenna was calculated using the following equation:

$$Power_{output,rectenna} = \frac{Power_{output,requirement}}{\eta_{rectenna}\eta_{stepdown}} \tag{12}$$

The efficiency of the rectenna is based upon the transmission frequency and the values were gathered from a literature review [20] [23] [24] . Next the area required to generate that power output based upon the rectenna's assumed aperture efficiency (ϵ_A) was determined with the equation below. The aperture efficiency is dependent on the transmission frequency and accounts for some interference effects between the rectenna's dipoles.

$$A_{rectenna} = \frac{Power_{output,rectenna}}{\Phi_r \epsilon_A} \tag{13}$$

Lastly, the mass of the rectenna can be found by multiplying the area by its specific mass. The rectenna was assumed to have an areal mass of 1.8 kg/m^2 [20] [23].

The final unique components to be sized for the RF Power Beaming system are the microwave generators. The previously mentioned NASA studies along with the study performed by Kerslake recommend the use of magnetrons for the microwave generators for several reasons [3] [27]. First, magnetrons are extremely well developed and understood pieces of technologies as they have been used in a variety of applications since their invention in the 1950's including the household microwave oven. Second, they have extremely long service lives even when operated continuously which is crucial for a power system. Lastly, they have high conversion efficiencies compared to other devices while also having low specific mass (kg/kW). A review of the leading industrial microwave generators was performed to determine their attributes needed for the studies. The results are listed in Table 2 [20] [23][31]. For sizing purposes, it was assumed that each magnetron would output 10 kW of power and due to the high voltage requirements each magnetron requires its own DDCU. The mass of the magnetrons are found by multiplying the calculated transmitted power requirement by the specific mass listed in the table. The same method can be done to find total heat generated by the magnetrons using the DC-to-RF conversion efficiencies.

Table 2 Magnetron Performance Attributes for Frequencies Studied [20] [23][31]

	2.45 GHz	5.8 GHz	10.0 GHz
Specific Mass (kg/kW)	3.4	2.5	1.2
DC-to-RF Conversion Efficiency	75%	50%	35%
Operating Voltage (V)	7800	8800	9400

E. Optical Beaming Sizing

A schematic of the optical power beaming system is shown by Figure 11 . Two scenarios will be analyzed in this section: fiber based and diode based lasers. The optical power beaming system is modeled for each scenario. Algorithm

7 highlights the process for sizing components and analyzing performance.

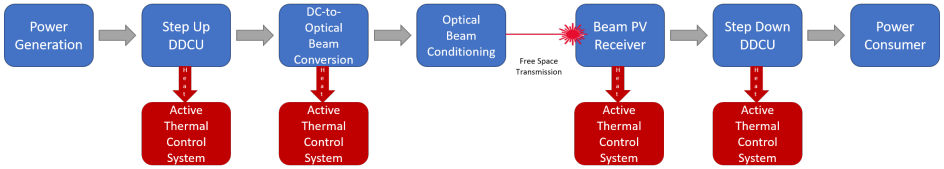

Fig. 11 Functional Decomposition of a Lunar Optical Beaming Power Distribution System.

Algorithm 7: Sizing the Optical Power Beaming System

Input: powerRequired, transmissionDistance
Output: Mass breakdown, efficiency breakdown
for *diodeLaser and fiberLaser* **do**
  while |*powerRequired - powerOutput*| > *1E-3* **do**
    Size the initial power conditioning and thermal control system;
    Size the laser and thermal control system;
    Size the optical conditioning;
    Size the receiver and thermal control system;
    Size the final power conditioning and thermal control system;
    Calculate overall system efficiency;
  end
end

1. Initial Power Conditioning

A DC-to-DC converter unit (DDCU) is used to condition the voltage for the laser beamforming component [7]. It is converted from 120 VDC to 50 VDC [3]. The DDCU generates heat due to some inefficiency, which is dissipated by sizing a thermal control system.

2. Beam Forming

The beam forming component is sized both for a diode-based laser and a fiber-based laser. The diode laser has an advantage in mass and efficiency. However, the fiber laser has an advantage in beam quality, requiring less mass for the optical conditioning and receiver. Both of these are modeled and compared to see how they affect the overall power transmission system mass. The modeling for each laser is primarily based on commercially available products.

In order to model the lasers, the efficiency and mass values are needed. The mass can be broken down into the laser head and the laser control unit. An additional 10% mass fraction is added for structural components. The thermal control system mass requires the dimensions of the laser, approximated as a rectangular prism and the operating temperature, modeled at 298 K. Additionally, the optical conditioning component requires the size of the laser beam being emitted. The necessary values are shown in Table 3 for each laser type.

3. Optical Conditioning

The optical beam needs to be conditioned to improve collimation over the long transmission distances. The beam generated by the diode laser has to additionally be circularized. The diode laser beam therefore requires a set of three lenses, while the fiber laser beam only requires one. The lenses being modeled are based on laser grade plano-convex cylinder lenses [34]. They are made from UV grade fused silica and have an optical reflectivity of 0.5% per surface. The volume of the lens is scaled with beam area at 3.43×10^{-3} m^3/m^2. Additionally, a 10% mass fraction for structure is added.

The optical conditioning system needs to output the beam diameter at the end of transmission in order to size the receiver. Equation 14 shows the calculation used for this, where the initial diameter refers to the diameter of the beam as

Table 3 Laser Sizing Parameters

	Diode [32]	**Fiber [33]**
Specific Mass of Laser Head	2.3 kg/kW	4 kg/kW
Specific Mass of Control Unit	25 kg/kW	40 kg/kW
Power Conversion Efficiency	55%	53%
Laser Beam Dimensions	5.66×10^{-3} m^2/kW	3.14×10^{-9} m^2/kW
System Size	0.155 m × 0.0586 m × 0.085 m/kW	0.1 m × 0.08 m × 0.08 m/kW

it passes through the lenses. Table 4 shows some key results for the study. The beam parameter product used for the diode laser is 100 mm-mrad and for the fiber laser is 1.9 mm-mrad.

$$finalDiameter(D_f) = \tan\left(\frac{beamParameterProduct(BPP)}{initialDiameter(D_0)}\right) \times transmissionDistance + D_0 \tag{14}$$

Table 4 Beam divergence from lens to receiver.

	Diode		**Fiber**	
	1 km	15 km	1 km	15 km
Initial Beam Diameter = 1 in	4 m	59 m	0.1 m	1.15 m
Initial Beam Diameter = 4 in	1 m	14.9 m	0.12 m	0.38 m
Initial Beam Diameter = 1 m	1.1 m	2.5 m	1.002 m	1.03 m

A beam diameter of 1 m is selected for the diode-based laser system and 1 inch for the fiber-based system across all scenarios. To achieve the required beam diameter for the lens, the beam is allowed to diverge from the laser emitter a specific distance until it passes through the lenses. The laser emitted beam diameter was checked to ensure that it is not larger than these selections at the highest power output.

4. Beam Receiver

InGaAs photovoltaic cells are selected for the receiver due to their high efficiency at the wavelengths corresponding to the optical beams. The receiver is modeled to have a power conversion efficiency of 42.6% at 1070 nm, the wavelength of the fiber-based optical beam [35]. The diode-based optical beam operates at a wavelength of 976 nm, so the receiver efficiency also needs to be found for that wavelength. Figure 12 shows the spectral response of an InGaAs cell across a range of wavelengths. Highlighted are the wavelengths for the lasers modeled. The spectral response is nearly identical for both wavelengths, so an efficiency of 42.6% is also used for the diode-based system.

An areal mass of 1.76 kg/m^2 is used along with a 10% mass fraction for additional structure. The area of the receiver is sized to be equal to the beam area when it reaches the receiver. For the thermal control system, the receiver is assumed to operate at 320 K. The receiver volume is approximated as a rectangular prism for the thermal control system model, where the receiving area is held constant but converted into a square. The depth of the receiver is then assumed to be 10% of the square's side length.

5. Final Power Conditioning

In order to regulate the output voltage of the receiver to be consistent for the consumer node, a solar array voltage output regulator (SAVOR) needs to be modeled. This is done using similar methods models as for the DDCU and other power electronics [7].

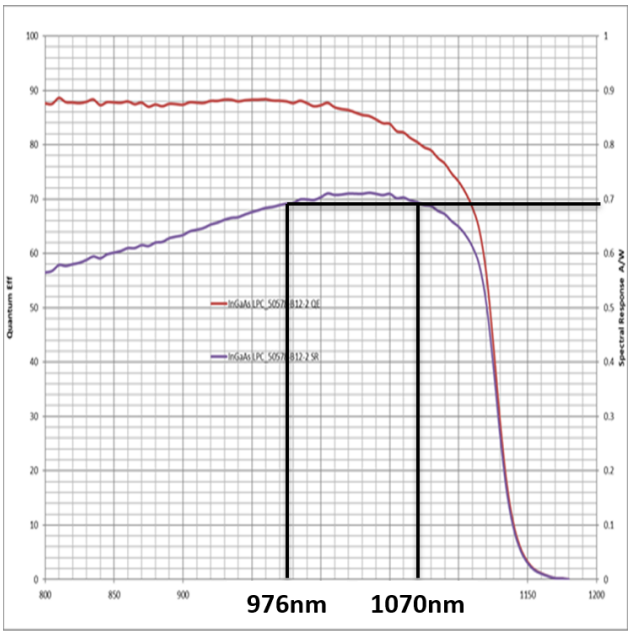

Fig. 12 Spectral response of an InGaAs pv cell [36].

IV. Analysis Overview and Setup

The goal of this analysis is to evaluate the performance of the defined Power Distribution Systems across a range of power levels and distances which are referred to as cases. The cases can best be shown by using a morphological matrix. In a morphological matrix, one value is selected from each row to create a single design point. The morphological matrix that defines the set of cases is shown in Table 5. An example of a single cases that would be ran is as follows: Optical Beaming at power level of 50 kW over a distance of 8 km. To fully cover the requirements of this study, 45 cases are required to be evaluated. In order to classify the performance of the systems in a standardized fashion across all 45 case studies, FOMs were developed that would allow for mission planners to make objective decisions and to compare different systems. The FOMs are listed in Table 1.

Table 5 Power Distribution System Study Morphological Matrix

Power Distribution System	DC Power Cables	RF Beaming	Optical Beaming		
Power provided to each Surface System	10 kW	25 kW	50 kW		
Transmission Distance to each Surface Systems	1 km	3 km	5 km	8 km	15 km

In order to manage the large number of cases and to handle future case studies in addition to the complexities of the sizing problems, the authors of the report elected to develop a modular computational code environment. Each of the algorithms discussed in the previous section were coded as Python 3.7 functions. A driver function was written that would evaluate each case from the morphological matrix and store the results into a database. Figure 13 shows the modular nature of the developed code base and the interactions between each module to enable the sizing of each PDS. Another advantage enabled by this choice is that designers can also easily execute additional studies to explore the impacts of component level assumptions on the entire system.

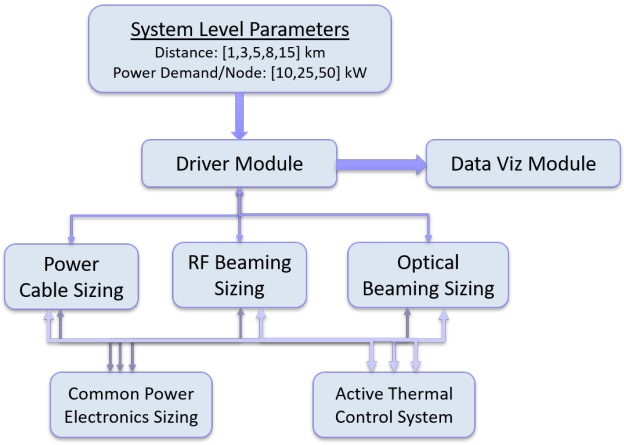

Fig. 13 Modular Python Code Environment.

V. Results

A. DC Power Cable Results

The primary reported result for this study is the landed mass. The cases outlined in the previous section were executed via the code and the following results were extracted for the DC Power Cables with the following design parameters: insulation thickness safety factor of 10 and a voltage drop limit of 5%. A breakdown of the results including component masses, transmission voltage, and conductor radius are shown for the 10 kW power cases in Table 6, the 25 kW power experiments in Table 7, and the 50 kW power cases in Table 8. The Conductor Bundle Mass is the total mass of the 6 conductors required for the system and the Insulation Bundle Mass is the total mass of the insulation for the transmission line bundle. Figure 14 compares the total system masses, including power generation, and visualizes the mass breakdown for all the cases analyzed in this study.

The power cables maintain a relatively high and consistent system electrical efficiency across all examined cases. The power cables had calculated efficiencies between 85 % and 87 %. This indicates that the system generates little waste heat as it transmits power. However, the high efficiency is a byproduct of the allowable 5% voltage drop requirement. To meet that requirement at the longer distances, the transmission voltage had to be increased nearly three-fold from the 1 km case. The voltage increases then had cascading effects on the overall mass of the system. The higher voltage required both a thicker conductor and insulation material. This in turn required a larger set of cable reels to be needed for deployment. Based on the results shown in the tables below, the deployment system mass at the 15 km transmission distance constitutes approximately 17% of the total mass whereas at the transmission distance of 1 km, it constitutes approximately 7%. When both increases are combined together, a quadratic relation between transmission distance and system mass can be observed. It should be noted that the masses of the other components are nearly invariant with regards to distance and scale proportionally with the power requirement which is in line with the results determined by Metcalf [7].

Table 6 Results for DC Power Cables at 10 kW Power Requirement.

Transmission Distance	1 km	3 km	5 km	8 km	15 km
Power Distribution System Mass	729.086 kg	1960.128 kg	3670.9	6856.077 kg	17660.566 kg
Power Input Required	11.726 kW	11.726 kW	11.726 kW	11.726 kW kg	11.726 kW
System Power Efficiency	85.3%	85.3%	85.3%	85.3%	85.3%
Transmission Voltage	1250 V	2000 V	2500 V	3250 V	4250 V
Conductor Radius	1.29 mm	1.31 mm	1.34 mm	1.304 mm	1.364 mm
Insulation Thickness	0.738 mm	1.181 mm	1.477 mm	1.919 mm	2.51 mm
Total System Mass with VSATs	1022.23 kg	2253.27 kg	3964.14 kg	7149.2 kg	17953.71 kg
Component Mass Breakdown					
Step Up DDCU	73.584 kg	73.475 kg	73.5 kg	73.593 kg	73.778 kg
Step Up DDCU ATCS	7.091 kg	7.084 kg	7.085 kg	7.092 kg	7.103 kg
Conductor Bundle	307.78 kg	945.42 kg	1668.9 kg	2517.48 kg	5160.59 kg
Insulation Bundle	110.5 kg	606.1 kg	1386.43 kg	3136.54 kg	8895.74 kg
Step Down DDCU	94.308 kg	94.233 kg	94.32 kg	94.485 kg	94.739 kg
Step Down DDCU ATCS	8.377 kg	8.373 kg	8.378 kg	8.388 kg	8.403 kg
Deployment System	97.367 kg	138.702 kg	270.36 kg	726.624 kg	2708.19 kg
Support Structures	9.17 kg	9.17 kg	9.172	9.178 kg	9.2 kg
VSAT Mass	293.14 kg	293.14 kg	293.14 kg	293.14 kg	293.14 kg

Table 7 Results for DC Power Cables at 25 kW Power Requirement.

Transmission Distance	1 km	3 km	5 km	8 km	15 km
Power Distribution System Mass	954.2573 kg	2714.196 kg	5395.178 kg	10856.29 kg	28292.985 kg
Power Input Required	28.736 kW	28.736 kW	28.736 kW	28.736 kW kg	28.736 kW
System Power Efficiency	87%	87%	87%	87%	87%
Transmission Voltage	2000 V	3250 V	4000 V	4500 V	5250 V
Conductor Radius	1.29 mm	1.29 mm	1.33 mm	1.49 mm	1.737 mm
Insulation Thickness	1.181 mm	1.92 mm	2.36 mm	2.66 mm	3.1 mm
Total System Mass with VSATs	1672.68 kg	3432.62 kg	6113.6 kg	11574.7 kg	29011.41 kg
Component Mass Breakdown					
Step Up DDCU	112.24 kg	112.47 kg	112.76 kg	112.98 kg	113.35 kg
Step Up DDCU ATCS	9.41 kg	9.42 kg	9.44 kg	9.45 kg	9.47 kg
Conductor Bundle	307.77 kg	923.33 kg	1633.66 kg	3269.77 kg	8376.43 kg
Insulation Bundle	200.4 kg	1168.73 kg	2675.12 kg	5400.42 kg	13796.13 kg
Step Down DDCU	163.52 kg	163.93 kg	164.3 kg	164.61 kg	165.08 kg
Step Down DDCU ATCS	12.14 kg	12.161 kg	12.18 kg	12.2 kg	12.2 kg
Deployment System	108.49 kg	204.653kg	557.34 kg	1438.392 kg	4696.66 kg
Support Structures	14.86 kg	14.89 kg	14.93 kg	14.96 kg	15.0 kg
VSAT Mass	718.4 kg	718.4 kg	718.4 kg	718.4 kg	718.4 kg

Table 8 Results for DC Power Cables at 50 kW Power Requirement.

Transmission Distance	1 km	3 km	5 km	8 km	15 km
Power Distribution System Mass	1284.351 kg	3877.325 kg	7871.47 kg	15739.75kg	40700.729 kg
Power Input Required	57.47 kW	57.47 kW	57.47 kW	57.47 kW	57.47 kW
System Power Efficiency	87%	87%	87%	87%	87%
Transmission Voltage	2750 V	4250 V	4750 V	5500 V	6250 V
Conductor Radius	1.32 mm	1.41 mm	1.59 mm	1.73 mm	2.07 mm
Insulation Thickness	1.62 mm	2.51 mm	2.8 mm	3.24 mm	3.69 mm
Total System Mass with VSATs	2721.19 kg	5314.17 kg	9308.32 kg	17176.59 kg	42137.57 kg
Component Mass Breakdown					
Step Up DDCU	171.48 kg	172.439 kg	172.86 kg	173.56 kg	174.33 kg
Step Up DDCU ATCS	12.5 kg	12.57 kg	12.6 kg	12.63 kg	12.67 kg
Conductor Bundle	322.25 kg	1093.81 kg	2359.1	4433.04 kg	11914.6 kg
Insulation Bundle	312.4 kg	1806.4 kg	3796.2 kg	7865.7 kg	19571.14 kg
Step Down DDCU	272.7219 kg	274.3043 kg	274.89 kg	275.81 kg	276.76 kg
Step Down DDCU ATCS	17.178 kg	17.246 kg	17.27 kg	17.31 kg	17.35 kg
Deployment System	120.35 kg	331.679 kg	902.89 kg	2322.784 kg	7135.51 kg
Support Structures	23.69 kg	23.82 kg	23.88 kg	23.97 kg	24.05 kg
VSAT Mass	1436.84 kg	1436.84 kg	1436.84 kg	1436.84 kg	1436.84 kg

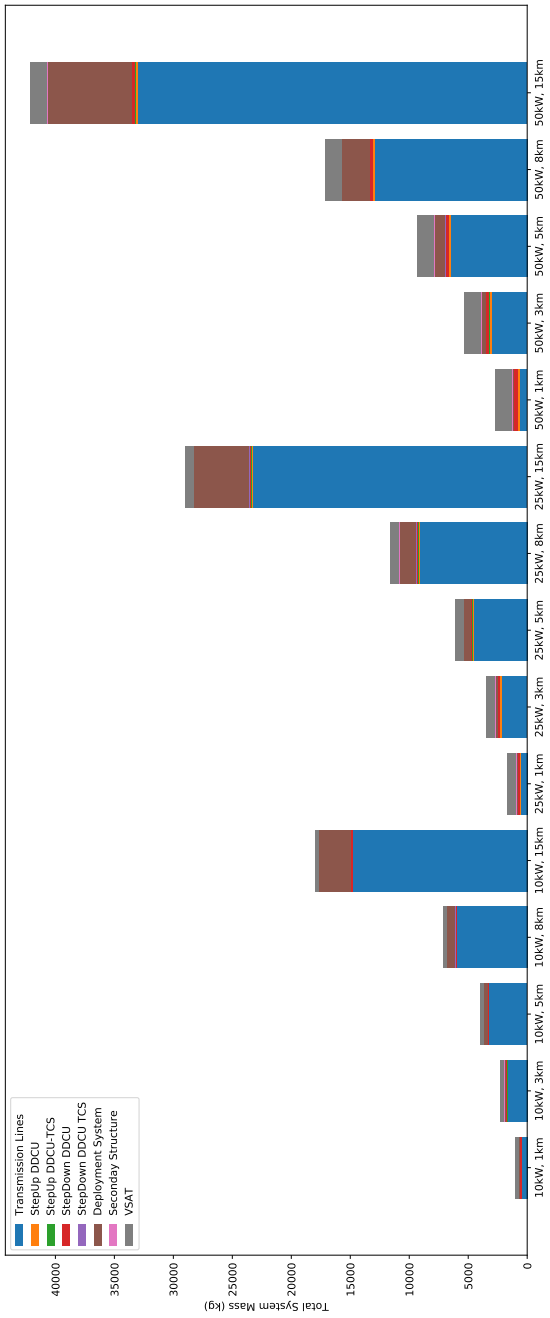

Fig. 14 Mass Breakdown of DC Power Cable Results.

B. RF Beaming Results

The primary reported result for this study is the landed mass. The experiment outlined in the previous section was ran through the code and the following results were extracted for the RF Power Beaming Systems. A breakdown of the results for the 2.45 GHz including component masses and transmission losses, and conductor radius are shown for the 10 kW power cases in Table 9, the 25 kW power cases in Table 10, and the 50 kW power cases in Table 11. Only the results for 2.45 GHz are shown in the tables below due its superior performance compared to the other 2 frequencies. The results of the 5.8 and 10 GHz analysis are available in the appendix. Figure 15 compares the total system masses and visualizes the mass breakdown for all the cases analyzed in this study.

The main thing to observe from the results is that the mass requirement for the VSATs is always greater then the mass of the transmission system. This is due to the significant power losses inherent for an RF based power distribution system. It can be observed that increasing the output power requirement while holding the transmission distance fixed, only increases the system's total mass by a small percentage. However; if distance is increased while holding the power requirement fixed, the system's total mass grows by several orders of magnitude. For example, at the 10 kW power requirement if the transmission distance is increased by a factor of 15, the total mass with VSATs increased by a factor of 210. The main driver for this is that free space transmission losses are directly related to the square of the distance. Therefore, in order to supply the required power despite the transmission losses, a large amount of power must be input into the beaming system. This results in a cascading effects that increases the radiated power requirement which require an increase in the number of microwave generators, Step Up DDCUs, and the ATCS to manage the increased heat load. Free space transmission losses can be reduced by increasing the transmission frequency; however, this would require substantial technology developments in all components. It should also be noted that for all cases except one (50 kW at 1 km) examined in this study, the transmission losses exceed the power output requirement.

Table 9 Results for RF Power beaming at 10 kW Power Requirement at 2.45 GHz.

Transmission Distance	1 km	3 km	5 km	8 km	15 km
Power Distribution System Mass	2274.44 kg	16718.26 kg	43682.83 kg	115181.89 kg	408372.02 kg
Power Input Required	188.39 kW	1692.71 kW	4491.27 kW	11916.67 kW	42371.8 kW
System Power Efficiency	5.31%	0.591%	0.223%	0.084%	0.024%
Transmission Losses	117.34 kW	1170.36 kW	3129.35 kW	8327.13 kW	29645.72 kW
Total System Mass with VSATs	6984.27 kg	59036.1 kg	155964.6 kg	413098.8 kg	1467667 kg
Component Mass Breakdown					
Step Up DDCUs	1130.9 kg	9612.8 kg	25445.75 kg	67451.4 kg	239674.76 kg
Step Up DDCU ATCS	118.92 kg	1010.85 kg	2675.77 kg	7092.9 kg	25203.26 kg
Microwave Generators Mass	476 kg	4046 kg	10710 kg	28390 kg	100878 kg
Microwave ATCS Mass	90.9 kg	804.6 kg	2133.5 kg	5659.3 kg	20118 kg
Transmission Antenna Mass	98.5 kg	884.4 kg	2346.5 kg	6226.1 kg	22137.82 kg
Rectenna Mass	249.37 kg	249.79 kg	261.51 kg	252.31 kg	249.46 kg
Step Down DDCU	100.17 kg	100.17 kg	100.17 kg	100.17 kg	100.17 kg
Step Down DDCU ATCS	9.53 kg	9.53 kg	9.53 kg	9.53 kg	9.53 kg
Support Structures	227.4 kg	1671.82 kg	4368.28 kg	11518.1 kg	40837.2 kg
VSAT Mass	4709.8 kg	42317 kg	112281.8 kg	297916.9 kg	1059295 kg

Table 10 Results for RF Power beaming at 25 kW Power Requirement at 2.45 GHz.

Transmission Distance	1 km	3 km	5 km	8 km	15 km
Power Distribution System Mass	2737.1 kg	17042.7 kg	45786.7 kg	114414 kg	404439 kg
Power Input Required	186 kW	1674 kW	4665 kW	11789 kW	41919 kW
System Power Efficiency	5.365%	0.597%	0.21%	0.082%	0.024%
Transmission Losses	94.12 kW	1135.91 kW	3229.5 kW	8216.36 kW	29307.5 kW
Total System Mass with VSATs	6984.27 kg	59036.1 kg	155964 kg	413098 kg	1467667 kg
Component Mass Breakdown					
Step Up DDCUs	1130.9 kg	9532.1 kg	26415 kg	66724 kg	237089 kg
Step Up DDCU ATCS	118.9 kg	1002.3 kg	2777.7 kg	7016.4 kg	24931 kg
Microwave Generators Mass	476 kg	4012 kg	11118 kg	28084 kg	99790 kg
Microwave ATCS Mass	90.3 kg	796.5 kg	2215.8 kg	5598.8 kg	19903 kg
Transmission Antenna Mass	97.7 kg	875.48 kg	2437.61 kg	6159.7 kg	21901 kg
Rectenna Mass	630.2 kg	631.2 kg	629.3 kg	637.6 kg	630.4 kg
Step Down DDCU	178.42 kg	178.42 kg	178.42 kg	178.42 kg	178.42 kg
Step Down DDCU ATCS	14.6 kg	14.6 kg	14.6 kg	14.6 kg	14.6 kg
Support Structures	273.7 kg	1704.3 kg	4578.6 kg	11441.4 kg	40443.9694 kg
VSAT Mass	4709.82 kg	41866.5 kg	116638.4 kg	294739.6 kg	1047998

Table 11 Results for RF Power beaming at 50 kW Power Requirement at 2.45 GHz.

Transmission Distance	1 km	3 km	5 km	8 km	15 km
Power Distribution System Mass	3485 kg	17930 kg	44939 kg	116272 kg	409309 kg
Power Input Required	188.2 kW	1691.6 kW	4488 kW	11909 kW	42344 kW
System Power Efficiency	5.31%	0.591%	0.223%	0.084%	0.024%
Transmission Losses	59 kW	1111 kW	3069 kW	8263 kW	29568 kW
Total System Mass with VSATs	8191.9 kg	60221.1 kg	157149 kg	413999 kg	1467929 kg
Component Mass Breakdown					
Step Up DDCUs	1130.9 kg	9612.8 kg	25445.7 kg	67370 kg	239513 kg
Step Up DDCU ATCS	118.9 kg	1010.8 kg	2675.7 kg	7084.4 kg	25186 kg
Microwave Generators Mass	476 kg	4046 kg	10710 kg	28356 kg	100810 kg
Microwave ATCS Mass	90.9 kg	804.2 kg	2132.5 kg	5654.8 kg	20105 kg
Transmission Antenna Mass	98.5 kg	884.4 kg	2345.1 kg	6222.4 kg	22123.6 kg
Rectenna Mass	1247.68 kg	1249.7 kg	1308.4 kg	1262.4 kg	1248.17 kg
Step Down DDCU	300.3 kg	300.3 kg	300.3 kg	300.3 kg	300.3 kg
Step Down DDCU ATCS	21.74 kg	21.74 kg	21.74 kg	21.74 kg	21.74 kg
Support Structures	348.5 kg	1793 kg	4493 kg	11627 kg	40930.9 kg
VSAT Mass	4706.8 kg	42290.84 kg	112210 kg	297727 kg	1058620 kg

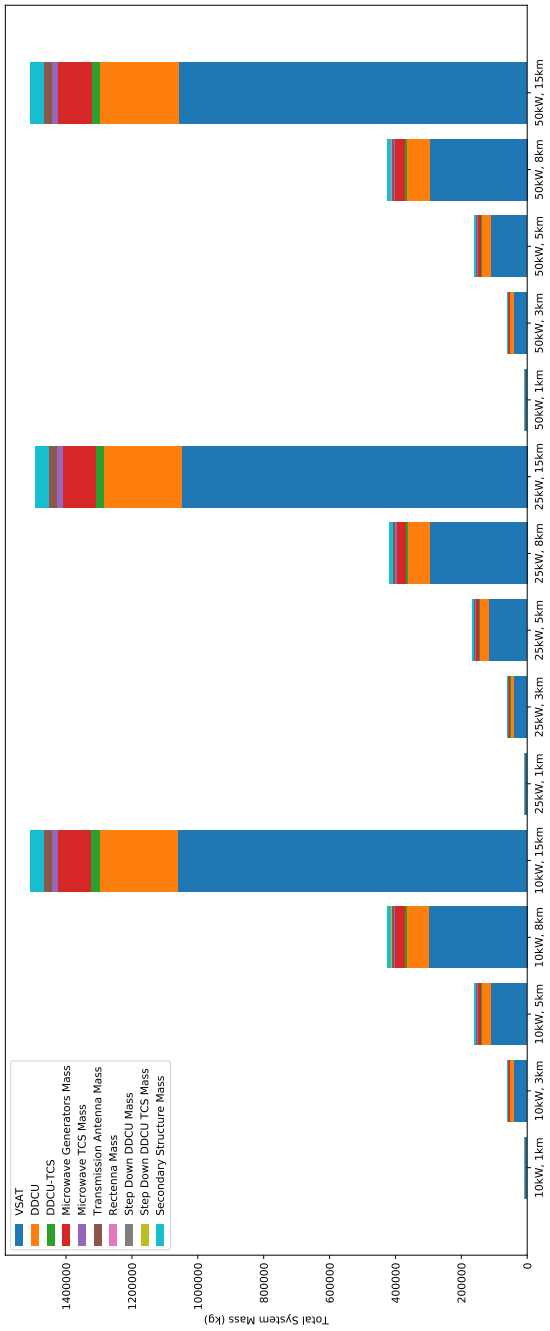

Fig. 15 Mass Breakdown of 2.45 GHz RF Power Beaming Results.

C. Optical Beaming Results

The primary result is the total landed mass. For the optical power beaming system, the largest contributor of the mass is the VSAT arrays due to the overall power conversion efficiency. The diode- and fiber-based optical systems both have efficiencies 21%, but the fiber-based systems are slightly less efficient. A breakdown of power losses is shown in Figure 16. The left side of the figure starts with all of the power collected by VSAT, then has arrows splitting off vertically for each of the sources of power loss. The power delivered to the consumer is the remainder of the arrow pointing to the right.

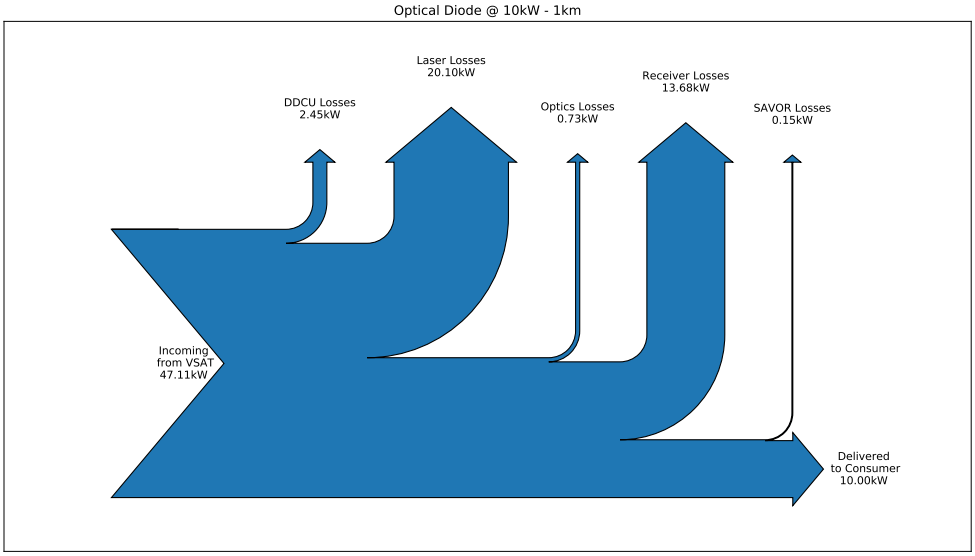

Fig. 16 Sankey diagram showing power losses for the 10kW - 1km - 1 node scenario. The width of the arrows is proportional to the power in that category.

The results of the simulations are shown in Tables 12-17. These tables include the total masses, efficiencies, and detailed mass breakdowns. The tables show that the masses of the optical power beaming systems increase slightly with increased distance, but increase significantly with increased power. Figure 17 shows the mass breakdown visually for each scenario. VSAT makes up the largest component of the mass, while the laser component constitutes the second largest mass.

Table 12 Results for the diode optical power beaming systems for the 10 kW power requirement.

Transmission Distance	1 km	3 km	5 km	8 km	15 km
Power Distribution System Mass	1163 kg	1169 kg	1176 kg	1188 kg	1226 kg
Power Input Required	47.1 kW	47.1 kW	47.1 kW	47.1 kW	47.1 kW
System Power Efficiency	21.2%	21.2%	21.2%	21.2%	21.2%
Total System Mass with VSATs	2340 kg	2346 kg	2353 kg	2366 kg	2403 kg
Component Mass Breakdown					
Step Up DDCUs	212 kg	212 kg	212 kg	212 kg	212 kg
Step Up DDCU ATCS	9.7 kg	9.7 kg	9.7 kg	9.7 kg	9.7 kg
Laser	738 kg	738 kg	738 kg	738 kg	738 kg
Laser ATCS	90.1 kg	90.1 kg	90.1 kg	90.1 kg	90.1 kg
Optics	19.6 kg	19.6 kg	19.6 kg	19.6 kg	19.6 kg
Receiver	1.8 kg	2.6 kg	3.4 kg	4.9 kg	9.5 kg
Receiver ATCS	39.5 kg	44.8 kg	51.0 kg	61.9 kg	94.8 kg
SAVOR	46.8 kg	46.8 kg	46.8 kg	46.8 kg	46.8 kg
SAVOR ATCS	5.4 kg	5.4 kg	5.4 kg	5.4 kg	5.4 kg
VSAT	1178 kg	1178 kg	1178 kg	1178 kg	1178 kg

Table 13 Results for the fiber optical power beaming systems for the 10 kW power requirement.

Transmission Distance	1 km	3 km	5 km	8 km	15 km
Power Distribution System Mass	1548 kg	1548 kg	1550 kg	1553 kg	1564 kg
Power Input Required	47.9 kW	47.9 kW	47.9 kW	47.9 kW	47.9 kW
System Power Efficiency	20.9%	20.9%	20.9%	20.9%	20.9%
Total System Mass with VSATs	2745 kg	2746 kg	2747 kg	2750 kg	2762 kg
Component Mass Breakdown					
Step Up DDCUs	215 kg	215 kg	215 kg	215 kg	215 kg
Step Up DDCU ATCS	9.79 kg	9.79 kg	9.79 kg	9.79 kg	9.79 kg
Laser	1165 kg	1165 kg	1165 kg	1165 kg	1165 kg
Laser ATCS	79.7 kg	79.7 kg	79.7 kg	79.7 kg	79.7 kg
Optics	0.004 kg	0.004 kg	0.004 kg	0.004 kg	0.004 kg
Receiver	0.015 kg	0.095 kg	0.24 kg	0.59 kg	2.0 kg
Receiver ATCS	25.9 kg	26.6 kg	27.7 kg	30.3 kg	40.7 kg
SAVOR	46.8 kg	46.8 kg	46.8 kg	46.8 kg	46.8 kg
SAVOR ATCS	5.4 kg	5.4 kg	5.4 kg	5.4 kg	5.4 kg
VSAT	1198 kg	1198 kg	1198 kg	1198 kg	1198 kg

Table 14 Results for the diode optical power beaming systems for the 25 kW power requirement.

Transmission Distance	1 km	3 km	5 km	8 km	15 km
Power Distribution System Mass	2628 kg	2634 kg	2641 kg	2654 kg	2691 kg
Power Input Required	117 kW	117 kW	117 kW	117 kW	117 kW
System Power Efficiency	21.5%	21.5%	21.5%	21.5%	21.5%
Total System Mass with VSATs	5541 kg	5547 kg	5554 kg	5566 kg	5604 kg
Component Mass Breakdown					
Step Up DDCUs	432 kg	432 kg	432 kg	432 kg	432 kg
Step Up DDCU ATCS	13.6 kg	13.6 kg	13.6 kg	13.6 kg	13.6 kg
Laser	1828 kg	1828 kg	1828 kg	1828 kg	1828 kg
Laser ATCS	199 kg	199 kg	199 kg	199 kg	199 kg
Optics	19.6 kg	19.6 kg	19.6 kg	19.6 kg	19.6 kg
Receiver	1.8 kg	2.6 kg	3.4 kg	4.9 kg	9.5 kg
Receiver ATCS	76.9 kg	82.2 kg	88.4 kg	99.3 kg	132 kg
SAVOR	51.1 kg	51.1 kg	51.1 kg	51.1 kg	51.1 kg
SAVOR ATCS	5.7 kg	5.7 kg	5.7 kg	5.7 kg	5.7 kg
VSAT	2913 kg	2913 kg	2913 kg	2913 kg	2913 kg

Table 15 Results for the fiber optical power beaming systems for the 25 kW power requirement.

Transmission Distance	1 km	3 km	5 km	8 km	15 km
Power Distribution System Mass	3643 kg	3643 kg	3645 kg	3648 kg	3660 kg
Power Input Required	119 kW	119 kW	119 kW	119 kW	119 kW
System Power Efficiency	21.1%	21.1%	21.1%	21.1%	21.1%
Total System Mass with VSATs	6605 kg	6606 kg	6607 kg	6610 kg	6622 kg
Component Mass Breakdown					
Step Up DDCUs	438 kg	438 kg	438 kg	438 kg	438 kg
Step Up DDCU ATCS	13.7 kg	13.7 kg	13.7 kg	13.7 kg	13.7 kg
Laser	2888 kg	2888 kg	2888 kg	2888 kg	2888 kg
Laser ATCS	183 kg	183 kg	183 kg	183 kg	183 kg
Optics	0.004 kg	0.004 kg	0.004 kg	0.004 kg	0.004 kg
Receiver	0.015 kg	0.095 kg	0.24 kg	0.59 kg	2.0 kg
Receiver ATCS	63.3 kg	64.0 kg	65.1 kg	67.8 kg	78.1 kg
SAVOR	51.1 kg	51.1 kg	51.1 kg	51.1 kg	51.1 kg
SAVOR ATCS	5.7 kg	5.7 kg	5.7 kg	5.7 kg	5.7 kg
VSAT	2963 kg	2963 kg	2963 kg	2963 kg	2963 kg

Table 16 Results for the diode optical power beaming systems for the 50 kW power requirement.

Transmission Distance	1 km	3 km	5 km	8 km	15 km
Power Distribution System Mass	5036 kg	5042 kg	5049 kg	5062 kg	5099 kg
Power Input Required	232 kW	232 kW	232 kW	232 kW	232 kW
System Power Efficiency	21.5%	21.5%	21.5%	21.5%	21.5%
Total System Mass with VSATs	10839 kg	10845 kg	10852 kg	10864 kg	10902 kg
Component Mass Breakdown					
Step Up DDCUs	779 kg	779 kg	779 kg	779 kg	779 kg
Step Up DDCU ATCS	19.9 kg	19.9 kg	19.9 kg	19.9 kg	19.9 kg
Laser	3645 kg	3645 kg	3645 kg	3645 kg	3645 kg
Laser ATCS	370 kg	370 kg	370 kg	370 kg	370 kg
Optics	19.6 kg	19.6 kg	19.6 kg	19.6 kg	19.6 kg
Receiver	1.8 kg	2.6 kg	3.4 kg	4.9 kg	9.5 kg
Receiver ATCS	139 kg	145 kg	151 kg	162 kg	195 kg
SAVOR	54.9 kg	54.9 kg	54.9 kg	54.9 kg	54.9 kg
SAVOR ATCS	6.0 kg	6.0 kg	6.0 kg	6.0 kg	6.0 kg
VSAT	5803 kg	5803 kg	5803 kg	5803 kg	5803 kg

Table 17 Results for the fiber optical power beaming systems for the 50 kW power requirement.

Transmission Distance	1 km	3 km	5 km	8 km	15 km
Power Distribution System Mass	7104 kg	7105 kg	7106 kg	7109 kg	7121 kg
Power Input Required	236 kW	236 kW	236 kW	236 kW	236 kW
System Power Efficiency	21.2%	21.2%	21.2%	21.2%	21.2%
Total System Mass with VSATs	13006 kg	13007 kg	13008kg	13011 kg	13023 kg
Component Mass Breakdown					
Step Up DDCUs	791 kg	791 kg	791 kg	791 kg	791 kg
Step Up DDCU ATCS	20.2 kg	20.2 kg	20.2 kg	20.2 kg	20.2 kg
Laser	5759 kg	5759 kg	5759 kg	5759 kg	5759 kg
Laser ATCS	348 kg	348 kg	348 kg	348 kg	348 kg
Optics	0.004 kg	0.004 kg	0.004 kg	0.004 kg	0.004 kg
Receiver	0.015 kg	0.095 kg	0.24 kg	0.59 kg	2.0 kg
Receiver ATCS	126 kg	126 kg	128 kg	130 kg	140 kg
SAVOR	54.9 kg	54.9 kg	54.9 kg	54.9 kg	54.9 kg
SAVOR ATCS	6.0 kg	6.0 kg	6.0 kg	6.0 kg	6.0 kg
VSAT	5902 kg	5902 kg	5902 kg	5902 kg	5902 kg

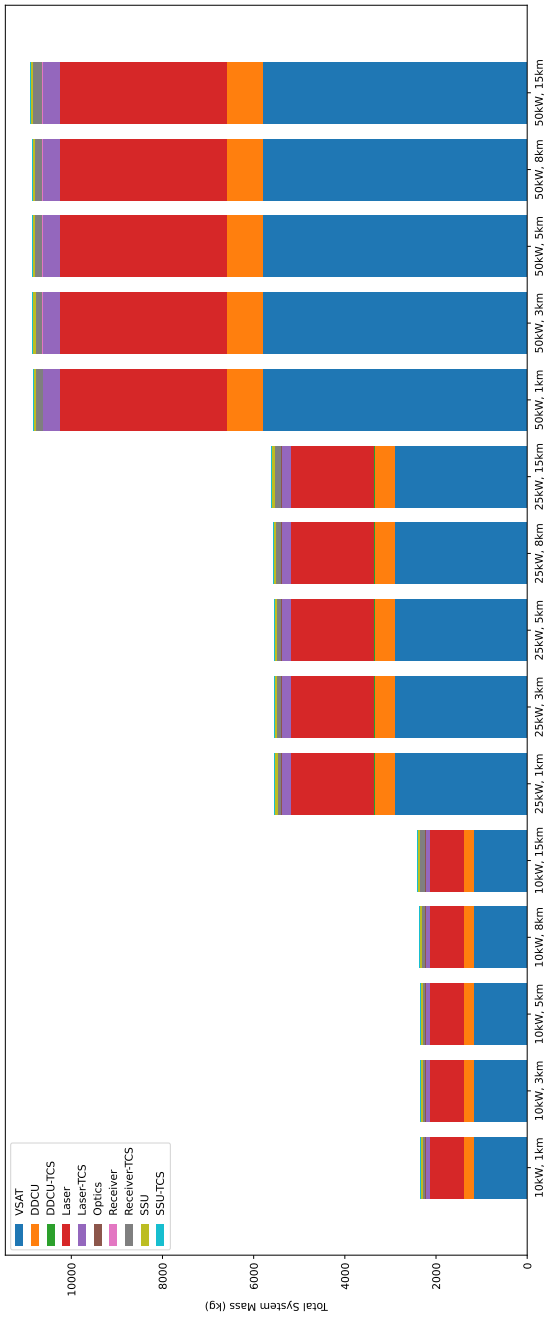

Fig. 17 Mass breakdown of the diode laser system for all scenarios.

Tables 18 and 19 show the sizing outputs for the diameters of the laser head, lens, and receiver for both the diode- and fiber-based systems. The fiber-based system allows for smaller lenses and a more compact receiver, which could provide deployment advantages especially at longer transmission distances over the diode-based system.

Table 18 Diameter sizing outputs of the diode-based optical systems in m.

	$10kW$			$25kW$			$50kW$		
	Laser Head	Lens	Receiver	Laser Head	Lens	Receiver	Laser Head	Lens	Receiver
$1km$	0.421	1	1.10	0.662	1	1.10	0.935	1	1.10
$3km$	0.421	1	1.30	0.662	1	1.30	0.935	1	1.30
$8km$	0.421	1	1.80	0.662	1	1.80	0.935	1	1.80
$15km$	0.421	1	2.50	0.662	1	2.50	0.935	1	2.50

Table 19 Diameter sizing outputs of the fiber-based optical systems in m.

	$10kW$			$25kW$			$50kW$		
	Laser Head	Lens	Receiver	Laser Head	Lens	Receiver	Laser Head	Lens	Receiver
$1km$	310×10^{-6}	0.0254	0.100	488×10^{-6}	0.0254	0.100	690×10^{-6}	0.0254	0.100
$3km$	310×10^{-6}	0.0254	0.250	488×10^{-6}	0.0254	0.250	690×10^{-6}	0.0254	0.250
$8km$	310×10^{-6}	0.0254	0.624	488×10^{-6}	0.0254	0.624	690×10^{-6}	0.0254	0.624
$15km$	310×10^{-6}	0.0254	1.15	488×10^{-6}	0.0254	1.15	690×10^{-6}	0.0254	1.15

D. Comparative Analysis

Figure 18 shows the mass-power regions in which a particular PDS has less total landed mass including the VSATs when compared to the alternatives. Total landed mass was the metric selected because it was calculated from the computational results and is the highest priority FOM listed in Table 1. This figure uses a contour map to project the three dimensional design space onto a two dimensional medium to enable decision makers to quickly determine the better performing system in terms of mass.

It can be observed from Figure 18 that the RF Power Beaming method never outperforms the other two options across the cases analyzed in this study. There do exist regions in which either the DC Power Cables or Optical Power Beaming outperform each other. For all distances below 3 km, it is more mass efficient to utilize power cables. As the distance is increased past 5 km, the optical power beaming begins to be the most mass efficient. Between 3 and 5 km exist the cross-over from power cables to optical beaming that is depending on the output power requirement. At lower output powers, optical beaming dominates this sub-region; however, as the power is increased, power cables dominate.

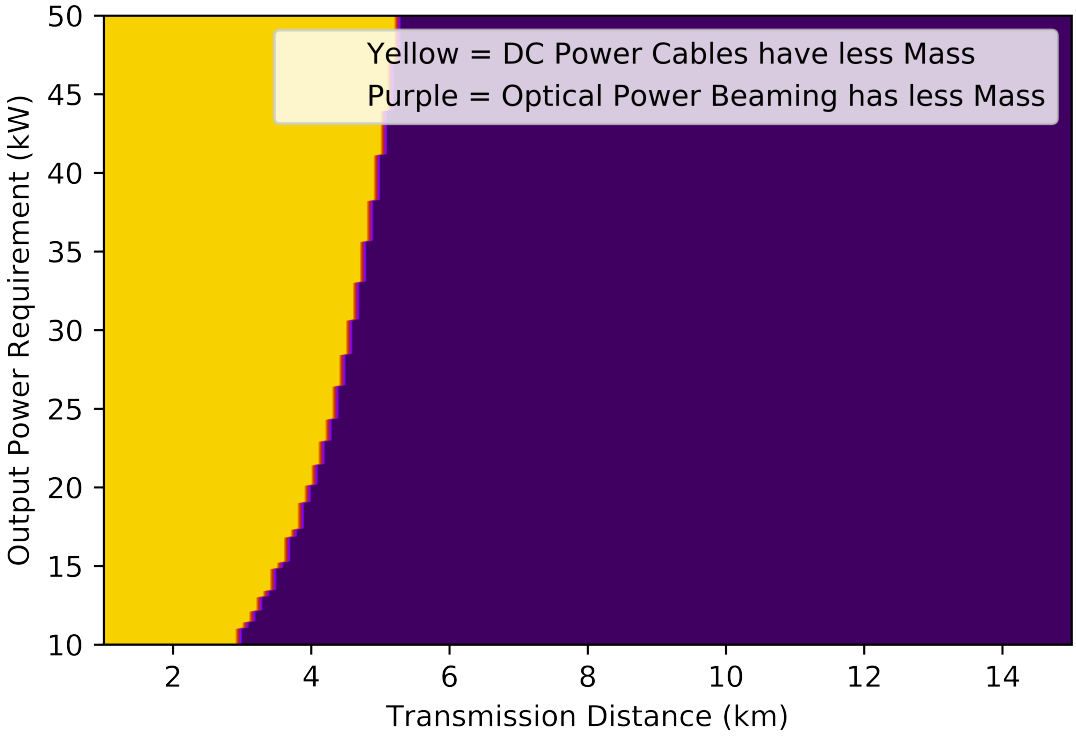

Fig. 18 Visual Representation of Mass Dominating PDS.

E. Qualitative Figures of Merit Analysis

The Reliability and Maintainability along with its Operational Flexibility are the two qualitative FOMs used to add additional levels to final performance evaluation for the distribution systems analyzed by this study, see Table 1. These additional discriminators are used by the mission planners to make the trade-offs between a system's landed mass and its operations. The following analysis and conclusions were drawn from work with SMEs and in-depth literature searches.

1. Reliability and Maintainability

As defined in Table 1, Reliability and Maintainability is the availability of the PDS to provide power across operational conditions. The evaluation of this FOM was done for each PDS in the study by analyzing the reliability and maintainability of each component.

All analyzed systems utilized two DDCUs (one Step-Up and one Step-Down) to provide the necessary power conditioning for transmission. These units were derived from the DDCUs utilized on the ISS which have design life of 15 years. To date, there have been no DDCU failures onboard the ISS; however, it is advised that a spare unit for each DDCU be included. Each DDCU is contained within an Orbital Replacement Unit which is a standardized component box that allows for both Astronauts and robots to easily perform maintenance operations. This analysis demonstrates that the DDCU components rate high for both reliability and maintainability.

Earth-based power cables have a typical life expectancy of 40-50 years with some having expectancy of 80 plus. It is assumed that the lunar power cables will be manufactured to the same standards, if not higher, and in addition to that there have been no power cable failures on-board the ISS which has a similar operating environment to the lunar surface. The cables were sized to in a manner to be 2-fault tolerant system due to the uncertainty surrounding the conductivity of the lunar regolith. Based on that research and reasoning, the DC Power cables rate high for reliability. The health of a power cable can be monitored using the current and voltage gathered from the DDCUs which would enable preventive maintenance to be carried out prior to a fault event. However, in the case of an electrical fault, instruments such as a

time-domain reflectometer can be used to determine the location of the fault. To restore the cable to operating conditions, the faulted portion of cable would need to cut out and a new segment spliced in. This is a time, man power, and tool intensive task. For this reason, the maintainability of power cables rates below moderate.

The RF power beaming system is untested PDS outside of case studies. It requires a complicated network of DDCUs, microwave generators, waveguides, antenna, and rectenna in order to transmit the power. Certain components are of little risk of failure, the waveguides and antenna, due to their passive design and a construction of aluminum; however, if any of them are damaged during transportation and deployment, the effect of the damage would not be observable till the system was fully deployed and energized. Also, the large number of DDCUs required for each of the microwave generators introduce additional points of failure which increases the number of spares required to ensure the system remains operational. While rated for a long operating life, upwards of 50,000 hours on earth, magnetrons have not been extensively tested in a lunar-like environment so their exact operating life is uncertain without further testing. Lastly, the rectenna array is also a passive circuit design with no moving parts; but it is sensitive to failures due to thermal stresses. There has not been a large-scale testing effort to quantify these effects on the operating life of the rectenna array. Therefore, the reliability of the RF power beaming system is rated as low. A compact design was assumed in the sizing meaning that the each magnetron is embedded with its waveguide into its antenna feed network meaning that if a magnetron was to fail it would require extensive man-hours to deenergize the array, disassemble the particular subarray, replace the failed unit, and then reassemble. The rectenna also faces issues with maintainability since each subarray is a printed circuit board. If more then one diode fails, it would require an entire replacement since its assumed the on-site facilities would not have the capabilites to fabricate a replacement. Based on those facts, the maintainability of the RF power beaming system is rated as low also.

Lastly, the optical power beaming system is untested on this scale but high power lasers are frequently deployed in manufacturing facilities which require high uptime. Also, the photovoltaic receivers are similar to the ones deployed for power generation. The fragile optics require special care during travel to the moon and deployment, but NASA has experience with deploying similar systems gained from space based telescopes which also have fragile optical systems. Additionally, the reliability could be improved by substituting the silica-based lenses with more durable Fresnel lenses. However, this would result in a loss of efficiency due to the higher reflectivity of Fresnel lenses. Although the diode-based system was found to be more efficient and less mass, the fiber-based system has higher reliability. The fiber laser has fewer fragile components since it consists of one fiber instead of a large array of diodes. In order to ensure high reliability of the system, its assumed that at least one set of spares will be required. Based on this line of reasoning, the reliability of this system is rated as moderate. The beam forming system is an entirely modular system which enables the ability to replace with moderate effort a failed unit. The lenses required for beam formation can be replaced with moderate effort assuming the system is designed appropriately. The same can be assumed for the photovoltaic receiver unit as NASA has experience with repairing and replacing solar arrays during space operations. Thus, the maintainability of the optical power beaming system is rated as moderate as well. Another advantage of the fiber-based system over the diode-based system would be that it requires a smaller receiver unit, which would be easier to maintain.

Table 20 below summarizes these results.

Table 20 Power Distribution System Reliability and Maintainability.

	Reliability	Maintainability
DC Power Cables	High	Moderate
RF Power Beaming	Low	Low
Optical Power Beaming	Moderate	Moderate

2. Operational Flexibility

Operational Flexibility is defined in this instance as the ability for the system to provide power over a wide rage of different operations for the end users. Stationary mission modules such has the lunar habitation module or the In-situ Resource Utilization module require no flexibility in operations as their deployment sites will be determined during the mission planning stages. However, other mission systems such as manned and unmanned lunar rovers will need to be mobile in order to fulfill their mission requirements. This means that the PDS assigned to each system must be flexible to support those operations.

DC Power cables require a physical connection between the source and user. In order to prevent damage to the cable and user, the user would need to have a mechanism in place to deploy and retract the cable as needed. As shown in the previous sections, the deployment systems become quite massive for longer distances that would be needed to enable exploration deep into Shackleton crater, a prime area for study during the Artemis missions [37]. The rover would also have to tow the deployment system possibility limiting its ability to traverse certain terrain. Therefore, the operational flexibility of DC Power cables is rated as low.

Both RF and Optical power beaming do not require a physical connection between source and user. The only requirement is that the receiver has line of sight to the transmitter. This then eliminates a significant operational hurdle posed by the DC Power cables. However, the size of the rectenna array required to enable long range power transmission for RF power beaming is prohibitively large. For that reason, RF Power beaming is rated as low. The receiver needed for optical power transmission could be integrated on a manned or unmanned rover. This would allow for the rover to have the freedom to explore any object of interest within the power transmission radius provided it can maintain line of sight which is not assumed to be an issue inside the crater if the transmitter is installed on the rim. Thus, the operational flexibility of the Optical power beaming system is rated as high.

Table 21 summarizes these results.

Table 21 Power Distribution System Operational Flexibility.

	Operational Flexibility
DC Power Cables	Low
RF Power Beaming	Low
Optical Power Beaming	High

VI. Areas for Future Work

For the DC Power Cables, furthering examining the impacts of the 5% allowed voltage drop requirement on the system mass and efficiency could benefit mission planners with defining the final system's requirement. In addition to that, further exploring the trade-offs surrounding the insulation safety factor would be beneficial. For the RF Power Beaming system, the use of other technologies in the various components should be explored. This includes items such as the microwave generators being based on solid-state or Klystron devices, higher frequency transmission components, different antenna, and advanced rectenna configurations. For the optical beaming, exploring different wavelengths for the laser combined with new materials for the PV receiver could be an avenue to study to determine its benefits. Along with exploring different component technologies, the computational model can be extended to include operational components to better evaluate the other FOMs. A Markov Chain analysis could be integrated to aide in determining system reliability. A lunar terrain model could also be incorporated to determine the performance of each system depending on its deployment location and to calculate line-of-sight issues for the power beaming systems.

VII. Conclusions

The goal of this study was achieved as a model was developed that evaluated the performance of power distribution systems on the lunar surfaces to support the planned Artemis Missions in the late 2020's. The three power distribution systems (DC Power Cables, RF Power Beaming, and Optical Power Beaming) were evaluated to determine their total required landed mass over distances from 1 km to 15 km at required power levels of 10 kW to 50 kW. The authors determined the distance-power regions in which each system had the lowest total landed mass. For distances under 3 km at all power levels, the DC Power Cables had the lowest mass. For distances greater then approximately 5 km at all power levels, the Optical Power Beaming had the lowest mass. In the transition region (3 km to approximately 5 km), Optical Power Beaming outperformed the Power Cables at the lower power levels but as the power level increased, the power cables outperformed the Optical Power Beaming. The DC Power Cables rated the highest on overall Reliability and Maintainability compared the other options with Optical Power Beaming being rated as moderate. However, the Optical Power Beaming is the superior option when it comes to enabling Operational Flexibility, rating high in the category while the other options were rated as low.

Appendix

The data obtained from the 5.8 GHz RF Beaming analysis is shown below.

Table 22 Results for RF Power beaming at 10 kW Power Requirement at 5.8 GHz.

Transmission Distance	1 km	3 km	5km	8 km	15 km
Total Transmission System Mass	2193.95 kg	15734.15 kg	41013 kg	108034.75 kg	382872.63 kg
Power Input Required	263.75 kW	2369.79 kW	6287.7 kW	16683.34 kW	59320.52 kW
System Power Efficiency	3.79%	0.422%	0.159%	0.060%	0.017%
Transmission Losses	115.43 kW	1168.451 kW	3127.4 kW	8325.23 kW	29643.82 kW
Total Mass with VSATs	8787.7 kg	74979.1 kg	198207 kg	525118 kg	1865886 kg
Component Mass Breakdown					
Step Up DDCUs	1130.922 kg	9612.84 kg	25445.7 kg	67451.44 kg	239674.8 kg
Step Up DDCU ATCS	118.9234 kg	1010.849 kg	2675.8 kg	7092.93 kg	25203.26 kg
Microwave Generators Mass	350 kg	2975 kg	7875 kg	20875 kg	74175 kg
Microwave ATCS Mass	176.8 kg	1575.9 kg	4180.15 kg	11089.7 kg	39427.5 kg
Transmission Antenna Mass	17.76 kg	159.51 kg	423.2 kg	1122.862 kg	3992.47 kg
Rectenna Mass	282.11 kg	282.58 kg	295.83 kg	285.44 kg	282.219 kg
Step Down DDCU	107.35 kg	107.35 kg	107.35 kg	107.35 kg	107.35 kg
Step Down DDCU ATCS	10.039 kg	10.039 kg	10.039 kg	10.039 kg	10.039 kg
Support Structures	219.39 kg	1573.42 kg	4101.3 kg	10803.47 kg	38287.26 kg
VSAT Mass	6593.75 kg	59244.9 kg	157194 kg	417083 kg	1483013 kg

Table 23 Results for RF Power beaming at 25 kW Power Requirement at 5.8 GHz.

Transmission Distance	1 km	3 km	5 km	8 km	15 km
Total Transmission System Mass	2716.1 kg	16126.56 kg	43071.8 kg	107404.8 kg	379276 kg
Power Input Required	260.94 kW	2344.523 kW	6531.7 kW	16505.42 kW	58687.87 kW
System Power Efficiency	9.485%	1.056%	0.383%	0.15%	0.042%
Transmission Losses	89.35 kW	1131.143 kW	3224.8 kW	8211.591 kW	29302.81 kW
Total Mass with VSATs	9239.522 kg	74739 kg	206365 kg	520040 kg	1846473 kg
Component Mass Breakdown					
Step Up DDCUs	1130.922 kg	9532.06 kg	26415.1 kg	66724.42 kg	237089.8 kg
Step Up DDCU ATCS	118.9234 kg	1002.354 kg	2777.7 kg	7016.48 kg	24931.44 kg
Microwave Generators Mass	350 kg	2950 kg	8175 kg	20650 kg	73735 kg
Microwave ATCS Mass	175.2 kg	1559.7 kg	4341.9 kg	10971.2 kg	39006.3 kg
Transmission Antenna Mass	17.63 kg	157.89 kg	439.6 kg	1110.883 kg	3949.81 kg
Rectenna Mass	712.87 kg	714.06 kg	711.9 kg	721.28 kg	713.15 kg
Step Down DDCU	194.83 kg	194.83 kg	194.83 kg	194.83 kg	194.83 kg
Step Down DDCU ATCS	15.67 kg	15.67 kg	15.67 kg	15.67 kg	15.67 kg
Support Structures	271.61 kg	1612.66 kg	4307.18	10740.5 kg	37927.6 kg
VSAT Generation Mass	6523.4 kg	58613.1 kg	1632934 kg	412635 kg	1467197 kg

Table 24 Results for RF Power beaming at 50 kW Power Requirement at 5.8 GHz.

Transmission Distance	1 km	3 km	5 km	8 km	15 km
Total Transmission System Mass	3560.71 kg	17102.02 kg	42432.3 kg	109292 kg	383983.5 kg
Power Input Required	263.5821 kW	2368.287 kW	6283.771	16672.72 kW	59282.72 kW
System Power Efficiency	18.97%	2.11%	0.796%	0.3%	0.084%
Transmission Losses	49.55 kW	1101.91 kW	3059.6 kW	8254.121 kW	29599.12 kW
Total Mass with VSATs	10150.26 kg	76309 kg	199526 kg	526109 kg	1866051 kg
Component Mass Breakdown					
Step Up DDCUs	1130.922 kg	9612.84 kg	25445.7 kg	67370.66 kg	239513.2 kg
Step Up DDCU ATCS	118.9234 kg	1010.849 kg	2675.7 kg	7084.435 kg	25186.27 kg
Microwave Generators Mass	350 kg	2975 kg	7875 kg	20850 kg	74125 kg
Microwave ATCS Mass	176.7 kg	1575.1 kg	4177.9 kg	11081.73 kg	39402 kg
Transmission Antenna Mass	17.77 kg	159.5 kg	422.9 kg	1122.19 kg	3989.917 kg
Rectenna Mass	1411.44 kg	1413.797 kg	1480.125 kg	1428.08 kg	1411.995 kg
Step Down DDCU	331.47 kg	331.47 kg	331.47 kg	331.47 kg	331.47 kg
Step Down DDCU ATCS	23.45 kg	23.45 kg	23.45 kg	23.45 kg	23.45 kg
Support Structures	356.07 kg	1710.2 kg	4243.2 kg	10929.2 kg	38398.35 kg
VSAT Generation Mass	6589.533 kg	59207.18 kg	157094 kg	416817. kg	1482068 kg

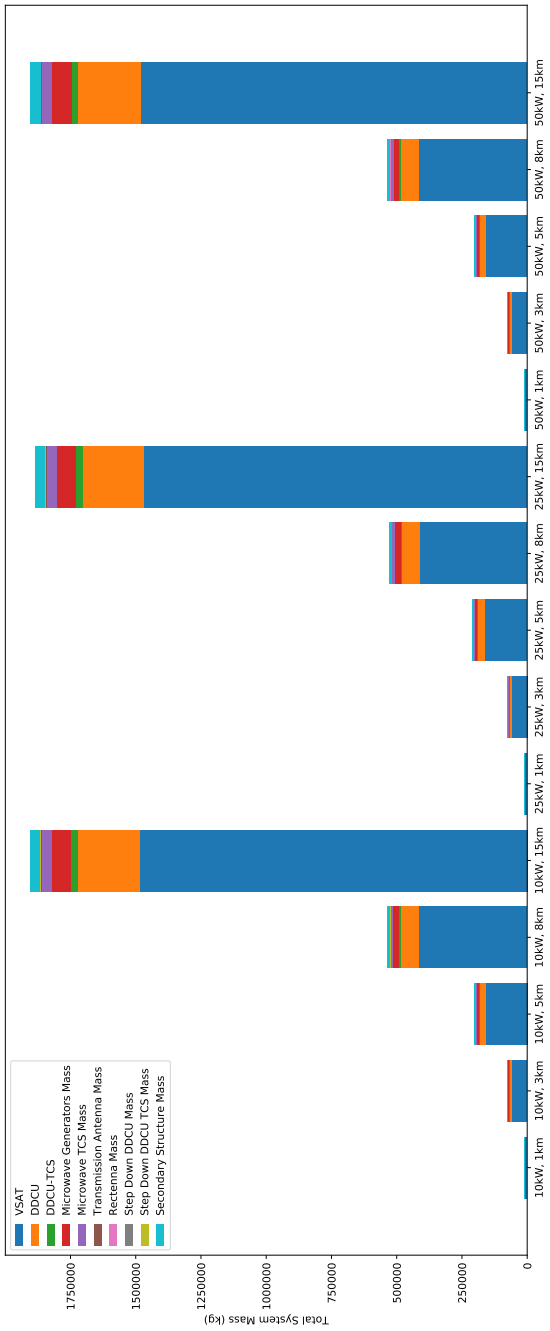

Fig. 19 Mass Breakdown of 5.8 GHz RF Power Beaming Results.

The data obtained from the 10 GHz RF Beaming analysis is shown below.

Table 25 Results for RF Power beaming at 10 kW Power Requirement at 10 GHz.

Transmission Distance	1 km	3 km	5km	8 km	15 km
Total Transmission System Mass	2202.6 kg	15312.7 kg	39785.65 kg	104659.5 kg	370706.5 kg
Power Input Required	376.7 kW	3385.425 kW	8982.5 kW	23833.35 kW	84743.6 kW
System Power Efficiency	2.65%	0.295%	0.111%	0.042%	0.012%
Transmission Losses	111.9 kW	1164.9 kW	3123.9 kW	8321.7 kW	29640.33 kW
Total Mass with VSATs	11622.3 kg	99948 kg	264349 kg	700493 kg	2489297 kg
Component Mass Breakdown					
Step Up DDCUs	1130.922 kg	9612.84 kg	25445.7 kg	67451.44 kg	239674.8 kg
Step Up DDCU ATCS	118.9234 kg	1002.354 kg	2777.7 kg	7016.48 kg	24931.44 kg
Microwave Generators Mass	168 kg	1428 kg	3780 kg	10020 kg	35604 kg
Microwave ATCS Mass	305.6 kg	2733 kg	7250.1 kg	19235 kg	68390.3 kg
Transmission Antenna Mass	6.056 kg	54.37 kg	144.25 kg	382.754 kg	1360.93 kg
Rectenna Mass	341.9 kg	342.5 kg	358.6 kg	345.99 kg	342.1 kg
Step Down DDCU	120.25 kg	120.25 kg	120.25 kg	120.25 kg	120.25 kg
Step Down DDCU ATCS	10.92 kg	10.92 kg	10.92 kg	10.92 kg	10.92 kg
Support Structures	220.26 kg	1531.3 kg	3978.5 kg	10465 kg	37070 kg
VSAT Mass	9419.6 kg	84635 kg	224563 kg	595833 kg	2118590 kg

Table 26 Results for RF Power beaming at 25 kW Power Requirement at 10 GHz.

Transmission Distance	1 km	3 km	5 km	8 km	15 km
Total Transmission System Mass	2832.5 kg	15816 kg	41902.5 kg	104177.6 kg	367354.2 kg
Power Input Required	372.77 kW	3349.3 kW	9331.1 kW	23579.2 kW	83839.9 kW
System Power Efficiency	6.707%	0.746%	0.268%	0.106%	0.03%
Transmission Losses	80.63 kW	1122.4 kW	3216.04 kW	8202.8 kW	29294.1 kW
Total Mass with VSATs	12151.6 kg	99549 kg	275179 kg	693565 kg	2463349 kg
Component Mass Breakdown					
Step Up DDCUs	1130.922 kg	9532.06 kg	26415.1 kg	66724.42 kg	237089.8 kg
Step Up DDCU ATCS	118.9234 kg	1002.354 kg	2777.7 kg	7016.48 kg	24931.44 kg
Microwave Generators Mass	168 kg	1416 kg	3924 kg	9912 kg	35220 kg
Microwave ATCS Mass	302.6 kg	2704.4 kg	7531 kg	19029.9 kg	67660.2 kg
Transmission Antenna Mass	6.01 kg	53.82 kg	149.8 kg	378.67 kg	1346.39 kg
Rectenna Mass	864.1 kg	865.53 kg	862.9 kg	874.27 kg	864.42 kg
Step Down DDCU	224.44 kg	224.44 kg	224.44 kg	224.44 kg	224.44 kg
Step Down DDCU ATCS	17.44 kg	17.44 kg	17.44 kg	17.44 kg	17.44 kg
Support Structures	283.25 kg	1581.6 kg	4190.25	10417.76 kg	36735.42 kg
VSAT Mass	9319.2 kg	83732 kg	233276 kg	589479 kg	2095995 kg

Table 27 Results for RF Power beaming at 50 kW Power Requirement at 10 GHz.

Transmission Distance	1 km	3 km	5 km	8 km	15 km
Total Transmission System Mass	3854.39 kg	16965.4 kg	41499.87 kg	106212.9 kg	372111.8 kg
Power Input Required	376.54 kW	3383.27 kW	8976.8	23818.17 kW	84689.6 kW
System Power Efficiency	13.28%	1.48%	0.557%	0.21%	0.059%
Transmission Losses	32.11 kW	1084.46 kW	3042.2 kW	8236.67 kW	29541.7 kW
Total Mass with VSATs	13268 kg	101547 kg	265920 kg	701667 kg	2489352 kg
Component Mass Breakdown					
Step Up DDCUs	1130.922 kg	9612.84 kg	25445.7 kg	67370.66 kg	239513.2 kg
Step Up DDCU ATCS	118.9234 kg	1010.849 kg	2675.7 kg	7084.435 kg	25186.27 kg
Microwave Generators Mass	168 kg	1428 kg	3780 kg	10008 kg	35580 kg
Microwave ATCS Mass	305.4 kg	2731 kg	7245.8 kg	19222 kg	68346.5 kg
Transmission Antenna Mass	6.056 kg	54.37 kg	144.16 kg	382.52 kg	1360.1 kg
Rectenna Mass	1710.8 kg	1713.7 kg	1794.1 kg	1731 kg	1711.5 kg
Step Down DDCU	387.8 kg	387.8 kg	387.8 kg	387.8 kg	387.8 kg
Step Down DDCU ATCS	26.42 kg	26.42 kg	26.42 kg	26.42 kg	26.42 kg
Support Structures	385.43 kg	1696.5 kg	4149.9 kg	10621.3 kg	37211.2 kg
VSAT Generation Mass	9413.6 kg	84581.7 kg	224420.4 kg	595454 kg	2117240 kg

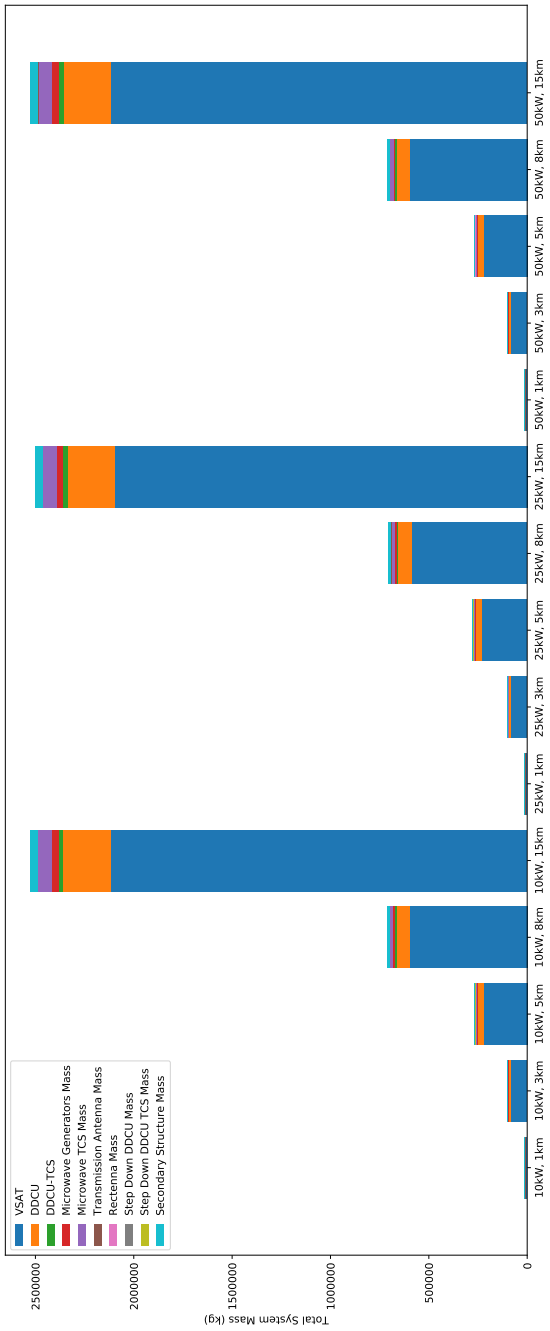

Fig. 20 Mass Breakdown of 10 GHz RF Power Beaming Results.

Acknowledgments

The work performed in this study was made available due to support and funding provided through NIA Task 601067.

References

[1] Spudis, P., Stockstill, K., Ockels, W., and Kruijff, M., "Physical environment of the lunar south pole from Clementine data: Implications for future exploration of the Moon," *Lunar and Planetary Science Conference*, Vol. 26, 1995.

[2] Fincannon, H., "Lunar Polar Illumination for Power Analysis," *6th International Energy Conversion Engineering Conference, IECEC*, Vol. -1, 2008, p. 5631. https://doi.org/10.2514/6.2008-5631.

[3] Kerslake, T. W., "Lunar Surface-to-Surface Power Transfer," *AIP Conference Proceedings*, Vol. 969, American Institute of Physics, 2008, pp. 466–473.

[4] References, E., "National Grid Overiew," , 2020. URL https://www.keystagewiki.com/index.php/National_Grid, accessed: 2020-08-04.

[5] Taylor, C., "Lunar Surface Solar Array Design Reference Mission, Concept of Operations, and Requirements," Tech. rep., NASA Langley Research Center, Hampton, Virginia, April 2020.

[6] Bruemmer, J. E., Williams, F. R., and Schmitz, G. V., "Efficient design in a DC to DC converter unit," *IECEC '02. 2002 37th Intersociety Energy Conversion Engineering Conference, 2002.*, 2002, pp. 56–60. https://doi.org/10.1109/IECEC.2002.1391974.

[7] Metcalf, K. J., "Power Management and Distribution (PMAD) Model Development," 2011.

[8] Wertz, J. R., Everett, D. F., and Puschell, J. J., *Space mission engineering: the new SMAD*, Microcosm Press, 2011.

[9] Birur, G. C., Siebes, G., and Swanson, T. D., "Spacecraft Thermal Control," *Encyclopedia of Physical Science and Technology*, edited by R. A. Meyers, Academic Press, New York, 2003, 3rd ed., pp. 485 – 505. https://doi.org/https://doi.org/10.1016/B0-12-227410-5/00900-5, URL http://www.sciencedirect.com/science/article/pii/B0122274105009005.

[10] Ku, J., "Introduction to Loop Heat Pipes," 2015.

[11] Stopar, J., "Near-Surface Temperatures Modeled at the Moon's South Pole (85°S to Pole)," , 2019. URL https://repository.hou.usra.edu/handle/20.500.11753/1336.

[12] Goncharov, K., Panin, Y., Balykin, M., and Khmelnitsky, A., "High thermal conductive carbon fiber radiators with controlled Loop Heat Pipes," 46th International Conference on Environmental Systems, 2016.

[13] Qu, Y., Wang, S., and Tian, Y., "A review of thermal performance in multiple evaporators loop heat pipe," *Applied Thermal Engineering*, Vol. 143, 2018, pp. 209–224.

[14] Deng, D., Liang, D., Tang, Y., Peng, J., Han, X., and Pan, M., "Evaluation of capillary performance of sintered porous wicks for loop heat pipe," *Experimental Thermal and Fluid Science*, Vol. 50, 2013, pp. 1–9.

[15] Gordon, L. B., "Electrical Transmission on the Lunar Surface Part I—DC Transmission," Tech. Rep. NASA/CR—2001-210759/PARTI, Auburn University, Auburn, Alabama, March 2001.

[16] Colozza, A., and Center, N. G. R., *Photovoltaic power system and power distribution demonstration for the Desert RATS program*, NASA technical memorandum, National Aeronautics and Space Administration, Glenn Research Center, 2012.

[17] "Winding Rope On a Winch," , 2020. URL https://samsonrope.com/resources/arborist/winding-rope-on-a-winch, accessed: 2020-08-02.

[18] *National electrical code handbook, 2020*, National Fire Protection Association, 2020.

[19] *ICEA S-75-381 Portable and Power Feeder Cables for Use in Mines and Similar Applications*, ICEA, 2014.

[20] McSpadden, J. O., and Mankins, J. C., "Space solar power programs and microwave wireless power transmission technology," *IEEE Microwave Magazine*, Vol. 3, No. 4, 2002, pp. 46–57.

[21] Brown, W. C., George, R. H., Heenan, N. I., and Wonson, R. C., "Microwave to DC converter," , March 25 1969. US Patent 3,434,678.

[22] Shaw, J. A., "Radiometry and the Friis transmission equation," *American Journal of Physics*, Vol. 81, No. 1, 2013, pp. 33–37. https://doi.org/10.1119/1.4755780, URL https://doi.org/10.1119/1.4755780.

[23] Jaffe, P., and McSpadden, J., "Energy Conversion and Transmission Modules for Space Solar Power," *Proceedings of the IEEE*, Vol. 101, No. 6, 2013, pp. 1424–1437.

[24] Dietz, R. H., "Workshop on Microwave Power Transmission and Reception. Workshop Paper Summaries," Tech. Rep. NASA-TM-84064, Lyndon B. Johnson Space Center, Houston, Texas, January 1980.

[25] Dickinson, R., "Evaluation of a microwave high-power reception-conversion array for wireless power transmission," Tech. Rep. NASA-CR-145625, Jet Propulsion Lab, Pasadena, CA, December 1975.

[26] Dickinson, R., "Microwave power transmitting phased array antenna research project," Tech. Rep. NASA-CR-157843, Jet Propulsion Lab, Pasadena, CA, December 1978.

[27] Maynard, O., Brown, W., Edwards, A., Haley, J., Meltz, G., Howell, J., and Nathan, A., "Microwave power transmission system studies. Volumes 1 through 4," Tech. Rep. NASA-CR-134886, Grumman Aerospace Corp, Bethpage, N. Y., December 1975.

[28] El Misilmani, H. M., Al-Husseini, M., and Mervat, M. Y., "Design of slotted waveguide antennas with low sidelobes for high power microwave applications," *Progress In Electromagnetics Research*, Vol. 56, 2015, pp. 15–28.

[29] Coburn, W., Litz, M., Miletta, J., Tesny, N., Dilks, L., and King, B., "A slotted-waveguide array for high-power microwave transmission," Tech. rep., ARMY RESEARCH LAB ADELPHI MD, 2001.

[30] Pandey, A., "Slotted Waveguide Array Antenna," , Dec 2016. URL https://anilkrpandey.wordpress.com/2016/12/05/slotted-waveguide-array-antenna/.

[31] "2450 MHz Industrial Microwave Generators," , 2020. URL https://www.mksinst.com/f/2450-mhz-industrial-microwave-generators.

[32] "Highlight DD Series," Tech. rep., Coherent, Inc., 2020. URL www.coherent.com, accessed: 2020-08-20.

[33] "YLS-10000-ECO," Tech. rep., IPG Photonics Corporation, 2020. URL www.ipgphotonics.com, accessed: 2020-08-04.

[34] "Laser Grade Plano-Convex (PCX) Lenses," , 2020. URL www.edmundoptics.com, accessed: 2020-08-20.

[35] Suzuki, H., Yoshida, H., Kisara, K., Nakamura, T., and Imaizumi, M., "Structural design of laser-photovoltaic power converter," *2014 IEEE 40th Photovoltaic Specialist Conference (PVSC)*, IEEE, 2014, pp. 1834–1838.

[36] "Provided by Spectrolab, Inc." .

[37] "Artemis Plan: NASA's Lunar Exploration Program Overview," Tech. Rep. NP-2020-05-2853-HQ, National Aeronautics and Space Administration, September 2020.